
Lappeenrannan teknillinen korkeakoulu
Lappeenranta University of Technology

Arto Laari

Gas-liquid mass transfer in bubbly flow: Estimation of mass transfer, bubble size and reactor performance in various applications

Acta Universitatis
Lappeenrantaensis 229

ISBN 978-952-214-784-4 (PDF)

LAPPEENRANTA
UNIVERSITY OF TECHNOLOGY

Arto Laari

Gas-liquid mass transfer in bubbly flow: Estimation of mass transfer, bubble size and reactor performance in various applications

Thesis for the degree of Doctor of Science (Technology) to be presented with due permission for the public examination and criticism in the Auditorium 1383 at Lappeenranta University of Technology, Lappeenranta, Finland, on the 19th of December, 2005, at noon.

Acta Universitatis
Lappeenrantaensis
229

Supervisor

Professor Ilkka Turunen
Department of Chemical Technology
Lappeenranta University of Technology
Finland

Reviewers

Professor Geoffrey M. Evans
Department of Chemical Engineering
University of Newcastle
Australia

Dr Gabriel Wild, directeur de recherche
Département de Chimie Physique des Réactions ENSIC - CNRS
Ecole Nationale Supérieure des Industries Chimiques (INPL)
France

Opponent

Dr Gabriel Wild, directeur de recherche
Département de Chimie Physique des Réactions ENSIC - CNRS
Ecole Nationale Supérieure des Industries Chimiques (INPL)
France

Custos

Professor Ilkka Turunen
Department of Chemical Technology
Lappeenranta University of Technology
Finland

ISBN 952-214-139-9
ISSN 1456-4491

Lappeenrannan teknillinen yliopisto
Digipaino 2005

ABSTRACT

Arto Laari

Gas-liquid mass transfer in bubbly flow: Estimation of mass transfer, bubble size and reactor performance in various applications

Lappeenranta 2005
86 p.
Acta Universitatis Lappeenrantaensis 229
Diss. Lappeenranta University of Technology

ISBN 952-214-139-9 ISSN 1456-4491

Gas-liquid mass transfer is an important issue in the design and operation of many chemical unit operations. Despite its importance, the evaluation of gas-liquid mass transfer is not straightforward due to the complex nature of the phenomena involved. In this thesis gas-liquid mass transfer was evaluated in three different gas-liquid reactors in a traditional way by measuring the volumetric mass transfer coefficient (k_La). The studied reactors were a bubble column with a T-junction two-phase nozzle for gas dispersion, an industrial scale bubble column reactor for the oxidation of tetrahydroanthrahydroquinone and a concurrent downflow structured bed. The main drawback of this approach is that the obtained correlations give only the average volumetric mass transfer coefficient, which is dependent on average conditions. Moreover, the obtained correlations are valid only for the studied geometry and for the chemical system used in the measurements. In principle, a more fundamental approach is to estimate the interfacial area available for mass transfer from bubble size distributions obtained by solution of population balance equations. This approach has been used in this thesis by developing a population balance model for a bubble column together with phenomenological models for bubble breakage and coalescence. The parameters of the bubble breakage rate and coalescence rate models were estimated by comparing the measured and calculated bubble sizes. The coalescence models always have at least one experimental parameter. This is because the bubble coalescence depends on liquid composition in a way which is difficult to evaluate using known physical properties. The coalescence properties of some model solutions were evaluated by measuring the time that a bubble rests at the free liquid-gas interface before coalescing (the so-called persistence time or rest time). The measured persistence times range from 10 ms up to 15 s depending on the solution. The coalescence was never found to be instantaneous. The bubble oscillates up and down at the interface at least a couple of times before coalescence takes place. The measured persistence times were compared to coalescence times obtained by parameter fitting using measured bubble size distributions in a bubble column and a bubble column population balance model. For short persistence times, the persistence and coalescence times are in good agreement. For longer persistence times, however, the persistence times are at least an order of magnitude longer than the corresponding coalescence times from parameter fitting. This discrepancy may be attributed to the uncertainties concerning the estimation of energy dissipation rates, collision rates and mechanisms and contact times of the bubbles.

Keywords: bubble column; gas-liquid mass transfer; bubble size; bubble coalescence; persistence time

UDC 544.431.11 : 532.529

Acknowledgments

The research work presented in this thesis has been carried out in Lappeenranta University of Technology in the Laboratory of Chemical Engineering and in the Laboratory of Product and Process Development

I wish to express my sincere gratitude to my supervisors, Professor Ilkka Turunen, Professor (Emeritus) Seppo Palosaari and Professor Juha Kallas.

I am also very grateful to the reviewers of my thesis, Professor Geoffrey Evans from the University of Newcastle, Australia, and Professor Gabriel Wild from École Nationale Supérieure des Industries Chimiques (INPL), France.

My special thanks go to the colleagues who have participated in the work, to Mrs. Marjatta Piironen and to Mr. Pekka Ilmola from Kemira Oyj. I also thank Mr. Harri Markkula and Mr. Veli-Matti Tuokkuri for their valuable work.

I also wish to thank Mr. Peter Jones for linguistic checking.

For financial support I am grateful to the National Technology Agency of Finland (Tekes), Kemira Oyj, The Research Foundation of Kemira Oyj and The Research Foundation of Neste Oyj.

Finally, I am grateful to my parents for their full support during the preparation of this thesis.

Lappeenranta, December 2005

Arto Laari

List of publications

I. Laari, A., Kallas, J., Palosaari, S. (1997), Gas-liquid mass transfer in bubble columns with a T-junction nozzle for gas dispersion, *Chem. Eng. Technol.*, **20**, 550-556.

II. Laari, A., Turunen, I., Haario, H., Piironen, M. (2001), Modelling of concurrent bubble column for gas-liquid reactions: model selection and validation, 5th International Conference on Gas-Liquid and Gas-Liquid-Solid Reactor Engineering, 23-27 September, 2001 Melbourne, Australia, 10 pages.

III. Laari, A., Piironen, M., Turunen, I., Haario, H., von Scala, C. (2002), Gas Holdup and Gas-Liquid Mass Transfer in Catalytic Structured Bed. CHISA 2002, 15th International Congress of Chemical and Process Engineering, 25-29 August 2002, Praha, Czech Republic, 20 pages.

IV. Laari, A., Turunen, I. (2003), Experimental determination of bubble break-up and coalescence rates in a bubble column reactor, *Can. J. Chem. Eng.*, **84** (3-4), 395-401.

V. Laari, A., Turunen, I. (2005), Prediction of coalescence properties of gas bubbles in a gas-liquid reactor using persistence time measurements, *Chem. Eng. Res. Des.*, **83** (A7), 881-886.

The author's contribution to the publications:

The author carried out the modelling work and parameter estimation and wrote the articles, with the assistance of the co-authors, in all publications. The experimental work was carried out by the author in publications I, III and V.

Other related publications:

Hautaniemi, M., Kallas, J., Munter, R., Trapido, M., Laari, A. (1998), Modelling of Chlorophenol Treatment in Aqueous Solutions. 2. Ozonation under Basic Conditions, *Ozone: Sci. Eng.*, **20**, 283-302

Laari, A., Korhonen, S., Tuhkanen, T., Verenich, S. and Kallas, J. (1999), Ozonation and Wet Oxidation in the Treatment of Thermomechanical Pulp (TMP) Circulation Waters, *Wat. Sci. Tech.*, **40**, 51-58.

Laari, A., Korhonen, S., Kallas, J. and Tuhkanen, T. (2000), Selective Removal of Lipophilic Wood Extractives from Paper Mill Circulation Waters, *Ozone: Sci. Eng.*, **22**, 585-605.

Verenich, S., Laari, A. and Kallas, J. (2000), Wet oxidation of concentrated wastewaters of paper mills for water cycle closing, *Waste Management*, **20**, 287-293.

Laari, A., Korhonen, S., Tuhkanen, T., Kallas, J. (2001), The effect of hydrodynamic and operational parameters on the deactivation kinetics of microbes in paper machine circulation water by ozonation, International Ozone Association, Proceedings of 15th Ozone World Congress London, 11th-15th September 2001, Vol.1, 438-453.

Verenich, S., Laari, A., Korhonen, S., Tuhkanen, T., Edelmann, K., Bankier, S., Kallas, J. (2001), Comparison of Ozonation and Wet Oxidation for the Destruction of Lipofilic Wood Extractives from Paper Mill Circulation Waters, *Ozone: Sci. Eng.*, **23**, 401-409.

Verenich, S., Laari, A., Nissén, M., Kallas, J. (2001), Combination of Coagulation and Catalytic Wet Oxidation for the Treatment of Pulp and Paper Mill Effluents, *Wat. Sci. Tech.*, **44**, 145-152.

Verenich, S., Laari, A., Kallas, J. (2003), Parameter Estimation and Sensitivity Analysis of Lumped Kinetic Models for Wet Oxidation of Concentrated Wastewaters, *Ind. Eng. Chem. Res.*, **42**, 5091-5098.

Kuosa, M., Laari, A., Kallas, J., (2004), Determination of the Henry's coefficient and mass transfer for ozone in a bubble column at different pH values of water, *Ozone: Sci. Eng.*, **26**, 277-286.

Verenich, S., Roosalu, K., Hautaniemi, M., Laari, A., Kallas, J. (2005), Kinetic modeling of the promoted and unpromoted wet oxidation of debarking evaporation concentrates, *Chem. Eng. J.*, **108**, 101-108.

Gas-liquid mass transfer in bubbly flow: Estimation of mass transfer, bubble size and reactor performance in various applications.

List of symbols

A	interfacial area	, m^2
A_R	cross-sectional area of column	, m^2
A_H	Hamaker force	, N
a	specific interfacial area	, m^2/m^3
a_1, a_2, a_3	experimental parameters	, -
B_B	birth rate by breakage	, $1/m^3$ s
B_C	birth rate by coalescence	, $1/m^3$ s
b_1, b_2, b_3	experimental parameters	, -
C	experimental coalescence parameter in Equation (39)	, -
C_B	coefficient in Equation (82)	, -
c	concentration	, mol/m^3
c_m	measured oxygen concentration	, mol/m^3
c_1, c_2, c_3	experimental parameters	, -
c_4	coefficient in Equation (18)	, -
c_5	coefficient in Equation (7)	, -
c_f	increase coefficient of surface area defined by Equation (19)	, -
D	diffusivity	, m^2/s
D_Γ	surface diffusivity	, m^2/s
D_B	death rate by breakage	, $1/m^3$ s
D_C	death rate by coalescence	, $1/m^3$ s
d_b	bubble diameter	, m
$d_{b,max}$	maximum stable bubble size	, m
d_e	equivalent bubble size	, m
d_H	hydraulic diameter	, m
d_1	major axis	, m
d_2	minor axis	, m
d_{32}	Sauter mean bubble diameter	, m
E_G	gas phase dispersion coefficient	, m^2/s
E_L	liquid phase dispersion coefficient	, m^2/s
E_z	bubble dispersion coefficient	, m^2/s
$f_{b,V}$	bubble breakage volume fraction	, -
f_r	repulsive force generated by one molecule of adsorbate at the barrier	, N/mol
H_C	height of cell	, m
H_s	height of spouting section in column	, m
H_{tot}	total column height	, m
h	thickness of liquid film between bubbles	, m

h_0	initial film thickness	, m
h_f	final film thickness	, m
k_1	reaction rate coefficient	, m^3/mol s
k_L	liquid side mass transfer coefficient	, m/s
$k_L a$	volumetric mass transfer coefficient	,1/s
k_w	coefficient in Equation (14)	, -
L_N	nozzle length	, m
n	number of bubbles in the size range $v + dv$	,1/m^6
n_λ	number of eddies of size λ in size range $\lambda + d\lambda$	,1/m^6
$n_{i,k}$	correction term in the birth by breakage term	, -
N_C	number of cells	, -
N_{comp}	number of components	, -
N_e	number concentration of eddies	,1/m^3
N_i	bubble number concentration in size group i	,1/m^3
$\dot{N}$	molar flow	, mol/s
$\dot{N}_{abs,i}$	absorption rate of component i	, mol/s
$\dot{N}_{abs}$	reaction rate of component i	, mol/s
$\dot{N}_{G,i}^{(feed)}$	feed rate of component i in gas phase	, mol/s
$\dot{N}_{L,i}^{(feed)}$	feed rate of component i in liquid phase	, mol/s
$\dot{N}_{r,i}$	reaction rate of component i	, mol/s
P_{kin}	kinetic power	, W
P_Γ	dimensionless coalescence threshold	, -
p	pressure	, Pa
Δp_{diss}	pressure loss by dissipation	, Pa
Δp_{dyn}	dynamic pressure loss	, Pa
Δp_{stat}	static pressure loss	, Pa
R	gas constant	, J/mol K
R_b	radius of barrier ring	, m
r	bubble radius	, m
$r_{i,j}$	equivalent bubble radius defined by Equation (38)	, m
r_k	reaction rate	, mol/m^3 s
$S_{i,j}$	cross-sectional area between colliding bubbles of sizes i and j	, m^2
$S_{i,e}$	cross-sectional area between a colliding bubble and a turbulent eddy	, m^2
S_Γ	normalized standard deviation	, -
s	bubble form factor	, -
s_d	average distance between bubbles	, m
s_1, s_1, s_1, s_1	parameters in Equation (50)	, -

T	temperature	, K
t_C	coalescence time	, s
t_e	exposure time for mass transfer	, s
$t_{i,j}$	film thinning time required for film rupture	, s
$\bar{t}$	characteristic diffusion time	, -
U_G	superficial gas velocity	, m/s
$U_{L,N}$	liquid superficial velocity in nozzle	, m/s
u_b	bubble rise velocity	, m/s
u_c	critical velocity	, m/s
u_s	slip velocity	, m/s
$u_{t,e}$	turbulent velocity of eddies	, m/s
$u_{t,i}$	turbulent velocity of bubbles in size group i	, m/s
u_{wake}	wake velocity	, m/s
V_C	volume of cell	, m^3
V_{mix}	mixing volume	, m^3
V_R	reactor volume	, m^3
$\dot{V}$	volumetric flow rate	, m^3/s
v	bubble volume	, m^3
x_i	representative size, also grid/pivot point	, m^3
$x_{i,k}$, $x_{i,j}$	parameters defined by Equations (67) and (68)	, -
z	length coordinate	, m

Greek symbols

α	fraction of Γ_i that remains at the barrier ring after the displacement of adsorbate molecules to the barrier ring	, -
α_p	parameter in Equation (118)	, -
β_l	coefficient in Equation (18)	, -
β_p	parameter in Equation (118)	, -
$\beta(v', v)$	daughter bubble size probability function	, $1/m^3$
Γ_m	minimum adsorbate concentration at the barrier ring required to support the weight of the bubble	, mol/m^2
$\bar{\Gamma}_i$	mean value of Gibbs surface excess of the adsorbate	, mol/m^2
γ	liquid phase backflow ratio	, -
$\Delta_{\otimes}$	mean cell height in forward direction	, m
δ	backward/forward cell height ratio	, -
δ_K	Kronecker delta function	, -
ε	turbulent energy dissipation rate	, W/kg
ε_G	holdup of gas	, -

ε_p	holdup of packings	, -
η	correction term in the birth by coalescence term	, -
$\theta_{i,e}$	collision rate of bubbles in size group i with eddies	, $1/m^3$ s
$\theta_{i,j}$	collision rate between bubbles in size groups i and j	, $1/m^3$ s
κ_1	roots of the Bessel function of the first kind, order one	, -
λ	eddy size	, m
λ_{min}	minimum size of eddies in the inertial size range	, m
λ_B	breakage efficiency	, -
$\lambda_B^{(w)}$	breakage efficiency by wake model	, -
μ_G	dynamic gas viscosity	, kg/m s
μ_L	dynamic liquid viscosity	, kg/m s
ν	kinematic viscosity	, m^2/s
ξ	gas phase backflow ratio	, -
ξ_r	eddy to bubble size ratio	, -
ρ_G	gas density	, kg/m^3
ρ_L	liquid density	, kg/m^3
σ	interfacial tension	, N/m
σ_Γ	standard distribution in the deviation of Γ_i	, -
τ	dynamic pressure force	, N
$\tau_{i,j}$	contact time of colliding bubbles in size groups i and j	, s
τ_p	time lag of oxygen probe	, s
τ_R	dimensionless persistence time	, -
$\Omega_B(v',v)$	breakage rate from size v to size v'	, $1/m^3$ s
$\Omega_B(v_i)$	specific breakage rate of bubbles in size group i	, $1/m^3$ s
$\Omega_C(v_i,v_j)$	coalescence rate between bubbles of sizes v_i and v_j	, $1/m^3$ s

Coefficient of determination

$$R^2 = \left(1 - \sum_{i=1}^{n}(y_i - y_p)^2 / \sum_{i=1}^{n}(y_i - \bar{y}_p)^2\right) \times 100\%$$

Dimensionless numbers

$$Re = \frac{\rho_L d_b u_b}{\mu_L}$$ Reynolds number

$$Re_H = \frac{\rho_L d_H U_L}{\mu_L (1-\varepsilon_p)}$$ Reynolds number based on hydraulic diameter

$Ca = \frac{\mu_L u_b}{\sigma}$	Capillary number
$Eö = \frac{g\Delta\rho d_e^2}{\sigma}$	Eötvös number
$F = g\left(\frac{d_b^8 \rho_L^5}{\sigma \mu_L^4}\right)^{1/3}$	Flow number
$V_N = u_b\left(\frac{d_b^2 \rho_L^2}{\sigma \mu_L}\right)^{1/3}$	Velocity number
$T_S = \left(\frac{\sigma}{\rho_L}\right)^{2/5} \frac{1}{\varepsilon^{3/5}}$	Time scale
$L = \left(\frac{\sigma}{\rho_L}\right)^{3/5} \frac{1}{\varepsilon^{2/5}}$	Length scale
$We_c = \frac{\tau}{\sigma / d_{b,max}}\left(\frac{\rho_G}{\rho_L}\right)^{1/3}$	Critical Weber number

Subscripts

b	bubble
G	gas
H	hydraulic
L	liquid
p	packing

1. Introduction

A special case of multiphase flow called bubbly flow, defined in this thesis as a flow where dispersed bubbles are flowing in liquid, is encountered in numerous applications over a large number of industrial areas including the chemical and process industries, biological wastewater treatment and energy production. A combination of bubbly flow with interfacial mass transfer is usual in many applications. These applications include chemical reactors, such as bubble columns, gas-liquid mixed tanks, static mixer reactors, aerobic wastewater treatment plants, and mass transfer equipment, such as absorption and distillation plate towers. The geometry and hydrodynamic conditions can vary considerably in different applications, but the principal phenomenon, gas-liquid bubbly flow combined with interfacial mass transfer, is the same for all applications.

Traditional methods to estimate the mass transfer characteristics of such reactors are based on experimental measurement of gas holdup, volumetric mass transfer coefficient and bubble size, the so called "nonadjustable parameters" (Deckwer, 1992). Numerous studies have been presented (for example, Keitel and Onken, 1981; Linek and Vacek, 1981; Gibilaro et al., 1985; Linek and Sinkule, 1991; Linek, Sinkule and Benes, 1992; Linek et al., 1993; Lara Márques, Wild and Midoux, 1994) on different methods to measure these parameters including dynamic, steady-state and chemical methods. The main drawback of the traditional approach is that in many cases it is not possible to use the real chemical system or real process conditions, like temperature and pressure, because of insurmountable practical difficulties or because of safety risks involved. Instead, the measurements are often limited to model compounds and atmospheric conditions. Unfortunately, an unexpected deviation sometimes exists between the parameters measured with model compounds and the parameters that can be observed in a real system. Therefore, it is generally considered that the measured parameters involve a great deal of uncertainty and caution is needed when using the measured parameters or literature correlations in process design. The main cause for the uncertainty related to the nonadjustable parameters is the complex effect of liquid physical properties and composition on bubble size, surface mobility and mass transfer.

A more fundamental approach is to solve the bubble size distribution from bubble breakage and coalescence rates. Several theoretical breakage models (Luo and Svendsen, 1996; Lehr, Millies and Mewes, 2002; Wang, Wang and Jin, 2003) and coalescence models (for example, Prince and Blanch, 1990; Colella et al., 1999; Lehr and Mewes, 2001; Lehr, Millies and Mewes, 2002) have been presented in the literature. These models can be used to calculate the local bubble size distribution using local flow conditions. However, at the present time the coalescence and breakage of bubbles is not yet fully understood and more basic research is needed in this area. Bubble coalescence depends on liquid properties and composition in a way which is difficult to estimate without experimental work.

The principal goal of this thesis is to increase our knowledge about bubble breakage, bubble coalescence and interfacial mass transfer in bubbly flows. Population balances are used in this work to describe the variations in the bubble size distributions. The closure of population balances requires specific models for bubble breakage and coalescence. Some models presented in the literature are further developed or modified and the corresponding model parameters are estimated based on experimental data. Another goal of this work is to study gas-liquid mass transfer experimentally in some gas-liquid reactors by measuring the volumetric mass transfer coefficient. Special attention is focused on the reliability of the estimated parameters and advanced statistical methods are applied to study parameter identifiability. In recent years simulation of multiphase flows by Computational Fluid Dynamics (CFD) has developed fast. The benefits of using CFD in multiphase flows are obvious. The solution of CFD code is independent of geometry and the same code can be used for any type of system. Although multiphase CFD is not a topic in this thesis the developed methods can be directly utilized in CFD to calculate local bubble size and interfacial mass transfer.

2. Breakage of bubbles

Bubble size is an important parameter and in bubbly flow it controls gas holdup and interfacial mass transfer area. The estimation of bubble size is, however, difficult because of the complex nature of the phenomena involved. Bubble size in bubbly flow is governed by several factors. These include the way the gas is fed into the flow (gas dispersion devices), gas and liquid feed rates, the physical properties of the gas and liquid (density, viscosity), flow conditions, like the level of turbulence, and the liquid phase composition.

Essentially, bubble size is determined by a dynamic balance between bubble breakage and coalescence rates. Therefore, the most accurate method of estimating bubble size is the solution of the population balance equation including phenomenological models for bubble breakage and coalescence.

2.1 Maximum stable bubble size

In turbulent flow, turbulent pressure fluctuations tend to deform the bubbles. These deformations may eventually lead to bubble breakage. Surface tension forces, on the other hand, act to resist these deformations. The ratio of these forces is defined as the critical Weber number. Levich (1962) also considers the balance between the internal pressure force and capillary pressure force.

According to Levich (1962) the critical Weber number may be defined as

$$We_c = \frac{\tau}{\sigma/d_{b,max}} \left(\frac{\rho_G}{\rho_L} \right)^{1/3} \qquad (1)$$

The dynamic pressure force can be evaluated by

$$\tau = \rho_L u_{t,e}^2 \qquad (2)$$

In isotropic homogeneous turbulence, the turbulent velocity fluctuations depend on the energy dissipation rate per unit mass.

$$u_{t,e}^2 = 2(\varepsilon d_{b,max})^{2/3} \tag{3}$$

Maximum stable bubble size can be obtained by solving Equation (1) with respect to bubble size. The effect of viscosity was not included in the original work by Levich (1962). According to Walter and Blanch (1986), the maximum stable bubble size is also proportional to the viscosity ratio μ_L/μ_G.

$$d_{b,max} = We_c^{0.6} \frac{\sigma^{0.6}}{\rho_G^{0.2}\varepsilon^{0.4}} \left(\frac{\mu_L}{\mu_G}\right)^{0.1} \tag{4}$$

The value of the critical Weber number depends on physical properties and operating conditions. Different values have been proposed in the literature. Lin, Tsuchiya and Fan (1998) estimate it to be 0.70 at 72 °C and 1.36 at 27 °C. Hesketh et al. (1987) give a value of 1.1 for bubbles in horizontal tube flow and Prince and Blanch (1990) present a value of 2.3 for turbulent gas-liquid flow.

The effect of pressure and temperature on the maximum stable bubble size has been considered by Lin, Tsuchiya and Fan (1998). Increase in pressure will decrease maximum stable bubble size according to Equation (4) because of the increase in gas density. The bubble size will also decrease at higher temperatures because both surface tension and viscosity will decrease as temperature rises.

Evidence of the effect of pressure on the maximum stable bubble size presented in the literature is substantial (for example, Wilkinson, Haringa and van Dierendonck, 1994; Lau et al., 2004; Schäfer, Merten and Eigenberger, 2002; Lemoine, Behkish and Morsi, 2004). Based on experimental results, Schäfer, Merten and Eigenberger (2002) present the following table (Table 1) about the effects of physical properties and operating conditions on the maximum stable bubble size. The results correspond well with Equation (4).

Table 1. The effect [1]of physical properties and operating conditions on the maximum stable bubble size (Schäfer, Merten and Eigenberger, 2002).

Physical property or operating condition	Mechanism	Effect on maximum stable bubble size
$\rho_G \Uparrow$	Inertia forces $\Uparrow$	$d_{b,max} \Downarrow$
$\mu_L \Downarrow$	Turbulence $\Uparrow$	$d_{b,max} \Downarrow$
$\sigma \Downarrow$	Surface energy $\Downarrow$	$d_{b,max} \Downarrow$
$p \Uparrow$	$\rho_G \Uparrow$, $\mu_L \leftrightarrow$, $\sigma \downarrow$	$d_{b,max} \Downarrow$
$T \Uparrow$	$\rho_G \downarrow$, $\mu_L \Downarrow$, $\sigma \Downarrow$	$d_{b,max} \Downarrow$
$U_G \Uparrow$	Bubble density $\Uparrow$	$d_{b,max} \Uparrow$

[1] $\Uparrow$ increase, $\Downarrow$ decrease, $\downarrow$ minor decrease, $\leftrightarrow$ no effect

Equation (4) gives an estimate for the maximum size of bubble that can survive in a turbulent flow. However, bubble size may be smaller than the maximum stable size because of a low coalescence rate. It seems that the prevailing bubble size can only be estimated through population balances by balancing the breakage and coalescence rates.

2.2 Bubble breakage rate models

Bubble breakage is a dynamic process and in order to follow the evolution of bubble size distribution over time it is necessary to evaluate the bubble breakage rate.

Several breakage rate models have been proposed in the literature. Some of these models are semi-empirical, like the ones by Prince and Blanch (1990) and Colella et al. (1999). In these models at least one experimental parameter is required.

Some completely theoretical models have been also proposed in the literature by Luo and Svendsen (1996), Lehr, Millies and Mewes (2002), Hagesaether, Jakobsen and Svendsen (2002) and Wang, Wang and Jin (2003, 2004).

The original model by Luo and Svendsen (1996) is based on surface energy restriction. The kinetic energy bombarding the bubble interface must be higher than the increase in surface

energy caused by bubble breakage. As pointed out by Hagesaether, Jakobsen and Svendsen (2002) and Wang, Wang and Jin (2003, 2004), the model by Luo and Svendsen (1996) is inconsistent in the sense that it estimates an infinitely high probability of daughter bubbles when the size of the daughter bubble approaches zero in the daughter bubble size probability function. This is clearly physically unjustified, the probability should go to zero with zero size daughter bubbles. The original model by Luo and Svendsen was later improved by Hagesaether, Jakobsen and Svendsen (2002) by the addition of a restriction according to which the energy density, defined as surface energy divided by bubble volume, cannot increase in the bubble breakage. The model by Lehr, Millies and Mewes (2002), on the other hand, is based on capillary pressure restriction. The capillary pressure σ / r of small bubbles is very high and the dynamic pressure $0.5\rho_L u_\lambda^2$ of the colliding eddy must exceed the capillary pressure for the bubble to be able to break. The model by Wang, Wang and Jin (2003, 2004) includes both the surface energy and capillary pressure restrictions and is in this sense more fundamental.

It is difficult to distinguish between the proposed models because of a lack of reliable bubble size data, especially at high gas feed rates. Furthermore, all the discussed theoretical models, except the model by Colella et al., have the theoretical weakness that they do not include the effect of gas density.

A summary of the breakage models is presented below.

2.2.1 Breakage rate model based on critical bubble velocity

In the breakage rate model proposed by Prince and Blanch (1990) breakage of the bubble is caused by the collision of bubbles with turbulent eddies. Only some collisions lead to bubble breakage. Eddies that are responsible for bubble breakage are of a size similar or smaller than the bubbles. Eddies that are larger than the bubbles merely transport the bubbles, whereas eddies much smaller than the bubbles do not have enough energy to break the bubbles.

The specific breakage rate of a bubble is expressed as a product of the collision rate and breakage efficiency.

$$\Omega_{B,i} = \theta_{i,e}\lambda_B \tag{5}$$

The collision rate between the bubbles and eddies can be estimated from

$$\theta_{i,e} = N_i N_e S_{i,e}(u_{t,i}^2 + u_{t,e}^2)^{1/2} \tag{6}$$

The number of eddies of size between λ and $\lambda + d\lambda$, is according to Luo and Svendsen (1996)

$$n_\lambda = \frac{c_5(1-\varepsilon_G)}{\lambda^4} \tag{7}$$

where $c_5 \approx 0.82$.

The total number of eddies taking part in the breakage process can be evaluated assuming that eddies smaller than $0.2 \times d_b$ do not have enough energy to break the bubbles and eddies larger than d_b merely transport the bubbles (Prince and Blanch, 1990).

Hence, the concentration of eddies per unit volume in breakage is

$$N_e = \int_{0.2d_b}^{d_b} \frac{c_5(1-\varepsilon_G)}{\lambda^4} d\lambda = \frac{c_5(1-\varepsilon_G)124}{3d_b^3} \approx \frac{33.9(1-\varepsilon_G)}{d_b^3} \tag{8}$$

Breakage efficiency may be estimated from

$$\lambda_B = \exp\left(-\frac{u_c^2}{u_{t,e}^2}\right) \tag{9}$$

The critical bubble velocity can be estimated from the definition of the Weber number (Equation (1)), which gives the critical bubble velocity as

$$u_c = \left(\frac{We_c \sigma}{d_b \rho_L}\right)^{1/2} \tag{10}$$

Turbulent eddy velocity is estimated from Equation (3)

2.2.1 Breakage rate model based on bubble wake mechanism

Colella et al. (1999) have proposed a breakage rate model based on a bubble-bubble wake interaction mechanism. This mechanism differs from the usual bubble-turbulent eddy mechanism, which neglects the interaction between bubbles and wakes.

Breakage rate is assumed to be a product of bubble-wake collision frequency and breakage efficiency.

$$\Omega_{B,i} = \theta_{i,j}^{(w)} \lambda_i^{(w)} \tag{11}$$

The bubble-wake collision frequency is estimated from

$$\theta_{i,j}^{(w)} = N_i N_j u_{i,j}^{rel} \frac{V_{i,wake}}{s_d} \tag{12}$$

where V_i^{wake} is the volume of the wake of a bubble of size class i and s_d is the average distance between bubbles.

The volume of the wake is assumed to have a conical shape with the base defined by the major axis and with a height equal to 5 times the major axis.

$$V_{i,wake} = \frac{5}{12} \pi d_i^3 \tag{13}$$

Colella et al. (1999) have developed the following model for breakage efficiency. Bubble breakage may take place when the bubble is partly inside and partly outside of a wake created by another bubble. The bubble is sucked towards the in-wake region tending to break the bubble. The following expression can be developed

$$\lambda_{B,i}^{(w)} = k_w \sqrt{\frac{\rho_G}{\rho_L}} u_{wake,i} (s-1)^2 \tag{14}$$

where k_W is an experimental parameter.

The shape of the bubbles also affects the breakage efficiency. More elongated bubbles with $s > 1$ are more prone to breakage. The bubbles are assumed to be oblate ellipsoids. The ratio of the major axis d_1 to the minor axis d_2 can be expressed as a function of the Eötvös number (Clift, Grace and Weber, 1978)

$$s = \frac{d_1}{d_2} = 1 + 0.163 \text{Eö}^{0.757} \tag{15}$$

where the Eötvös number is defined as

$$\text{Eo} = \frac{g \Delta \rho d_e^2}{\sigma} \tag{16}$$

where d_e is the equivalent bubble size defined as

$$d_e = \sqrt{d_1 d_2} \tag{17}$$

An important point in the proposed model for breakage efficiency is that the breakage is dependent on gas density, which corresponds well with experimental results presented in the literature.

2.2.2 Breakage rate model based on surface energy restriction

Luo and Svendsen (1996) have developed a theoretical breakage rate model for breakage of drops or bubbles in a turbulent field. In the model, turbulence is assumed to be isotropic. Only binary breakage is considered. The breakage volume fraction is assumed to be stochastic. The occurrence of breakage is determined by the energy level of the arriving eddy. Only eddies of a length scale smaller than or equal to the particle diameter can induce particle oscillations.

The breakage rate of a particle of size d (or v) into sizes of vf_{BV} and $(1-vf_{BV})$ is given by the equation

$$\frac{\Omega_B(v',v)}{(1-\varepsilon_G)^n} = c_4\left(\frac{\varepsilon}{d^2}\right)^{1/3}\int_{\xi_{r,min}}^{1}\frac{(1+\xi_r)^2}{\xi_r^{11/3}}\exp\left(-\frac{12c_f\sigma}{\beta_1\rho_c\varepsilon^{2/3}d^{5/3}\xi_r^{11/3}}\right)d\xi_r \qquad (18)$$

where $\xi_{r,min} = \lambda_{min}/d$, $c_4 \approx 0.923$ and $\beta_1 \approx 2.05$.

The proposed equation for breakage rate is completely theoretical. It has no experimental parameters.

λ_{min} is the minimum size of eddies in the inertial subrange.

The increase coefficient of surface area, c_f, is defined as

$$c_f = f_{b,v}^{2/3} + (1-f_{b,v})^{2/3} - 1 \qquad (19)$$

where $f_{b,v} = \frac{v'}{v}$ is the breakage volume fraction calculated as the ratio of the smaller daughter bubble volume v' and the volume of the parent bubble v.

2.2.3 Breakage rate model based on capillary pressure restriction

Lehr, Millies and Mewes (2002) have presented a breakage model which is based on the capillary pressure constraint. Bubble breakage occurs if the dynamic pressure caused by the colliding eddy is higher than the capillary pressure of the daughter bubble size.

$$0.5\rho_L u_\lambda^2 \geq 2\frac{\sigma}{d'} \qquad (20)$$

where d' is the diameter of the daughter bubble.

The breakage rate from size v into size v' and (v – v') is given by

$$\Omega_B(v',v) = \int_{d'}^{d} \sqrt{2}\, c_5 \frac{\sigma}{\rho_L \varepsilon^{2/3} d'^4} \frac{(\lambda + d)^2}{\lambda^{13/3}} \exp\left(-\frac{2\sigma}{\rho_L \varepsilon^{2/3} d'} \frac{1}{\lambda^{2/3}} \right) d\lambda \tag{21}$$

where $c_5 \approx 0.8413$

Equation (21) can be split into the specific breakage rate and the daughter bubble size distribution

$$\Omega_B(v',v) = \Omega_B(v)\beta(v',v) \tag{22}$$

using dimensionless time and length scales.

$$T_S = \left(\frac{\sigma}{\rho_L} \right)^{2/5} \frac{1}{\varepsilon^{3/5}} \tag{23}$$

$$L = \left(\frac{\sigma}{\rho_L} \right)^{3/5} \frac{1}{\varepsilon^{2/5}} \tag{24}$$

The following equations are obtained for the dimensionless breakage rate and the daughter bubble size probability distribution.

$$\Omega^*_{B,i} = 0.5 d_i^{*5/3} \exp\left(-\frac{\sqrt{2}}{d_i^{*3}} \right) \tag{25}$$

$$\beta^*_{i,k} = \frac{6}{\pi^{3/2} d_k^{*3}} \frac{\exp\left\{ -\frac{9}{4} \left[\ln\left(2^{2/5} d_k^* \right) \right]^2 \right\}}{\left\{ 1 + \mathrm{erf}\left[\frac{3}{2} \ln\left(2^{1/15} d_i^* \right) \right] \right\}} \tag{26}$$

The dimensionless specific breakage rate, daughter size distribution and bubble size are defined as

$$\Omega^*_{B,i} = \Omega_{B,i}\, T_S \tag{27}$$

$$\beta^*_{i,k} = \beta_{i,k}\, L^3 \tag{28}$$

$$d_i^* = d_i/L \tag{29}$$

The shape of the daughter bubble size probability distribution is presented in Figure 1. One can see that for small bubbles the breakage for two equal sized bubbles is the most probable. For larger bubbles, however, breakage for one larger and one smaller bubble is more favourable. Also, one may notice that the probability approaches zero as the breakage fraction approaches zero with all mother bubble diameters. This result is reasonable as the production of infinitely small bubbles is not physically justified.

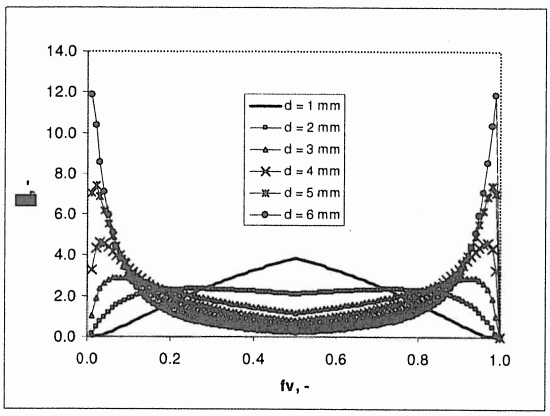

Figure 1. The shape of the daughter bubble size probability distribution predicted by the breakage model of Lehr, Millies and Mewes (2002). Physical properties of water and air at 293 K. Turbulent energy dissipation rate $\varepsilon = 0.1$ W/kg.

3. Bubble coalescence

In bubble coalescence, bubbles approach each other due to turbulence, different flow velocity or wake interaction and after contact coalesce to form a larger bubble. Despite its importance, coalescence phenomena are yet not well understood. Some models to estimate the coalescence rate have been proposed in the literature by Prince and Blanch (1990), Lehr and Mewes (2001), Lehr, Millies and Mewes (2002) and Kamp et al. (2001).

The coalescence of bubbles depends very much on the liquid composition. It is well-known that even very small amounts of impurities or presence of electrolytes (see Figure 3) in the liquid can change the coalescence properties dramatically. Evidence in the literature concerning the effect of liquid composition is very large (for example, Yagi and Yoshida, 1974; Oels et al., 1978; Keitel and Onken, 1982; Kelkar et al., 1983; Öztürk, Schumpe and Declwer, 1987; Jamialahmadi and Müller-Steinhagen, 1992; Del Pozo, Briens and Wild, 1994; Machoň et al., 1996).

3.1 Film thinning model

In the coalescence theory developed by Marrucci (1969), it is assumed that when bubbles are in contact a thin liquid film is left between the bubbles. This film thins due to drainage from the initial thickness to some critical thickness where film rupture takes place and the bubbles coalesce. Coalescence takes place if the contact time is longer than the time required for film drainage. The contact time depends on turbulence. If the film does not have enough time to drain, the bubbles are carried away by a turbulent eddy. When surface active compounds are accumulated on the gas-liquid surface they change the behavior of the liquid film. As the film between the bubbles stretches a concentration gradient is formed between the stretched film and the other parts of the interface. This generates surface active forces, which tend to oppose the film stretching and so increase the film thinning time. The liquid film thinning rate for equal sized bubbles can be expressed by

$$-\frac{dh}{dt}=\left\{\frac{8}{r^2\rho_L}\left[\frac{-4c}{RT}\left(\frac{d\sigma}{dc}\right)^2+h^2\left(\frac{2\sigma}{r}+\frac{A_H}{6\pi h^3}\right)\right]\right\}^{1/2} \tag{30}$$

where A_H is the Hamaker force.

Equation (30) includes Marrucci's coalescence parameter $c(d\sigma/dc)^2$. Since the gradient of surface tension with respect to concentration in the coalescence parameter has a power of two, the coalescence retardation effect is similar for compounds which increase or decrease surface tension. For example, the surface tension increases for electrolytes and decreases for surface-active compounds.

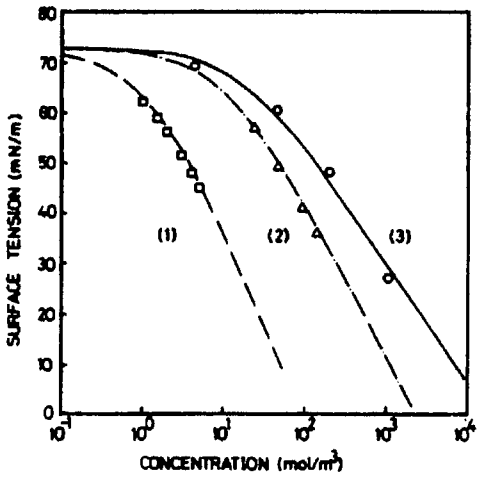

Figure 2. Effect of surface-active compounds on surface tension (Kim and Lee, 1987). (1) sodium layryl sulphate, (2) n-amyl alcohol, (3) 1-butanol.

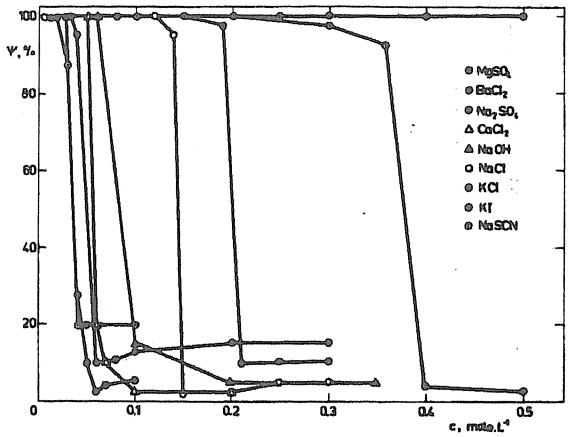

Figure 3. Effect of electrolyte concentration on coalescence probability (Zahradnik et al., 1995).

Theoretically, the coalescence parameter and the coalescence properties of a solution can be estimated by measuring the surface tension of the solution with different solute concentrations (see Figure 2). In practice, this is not easy because the concentration of surface-active compounds required to change the coalescence properties can be very low. In addition, the solution is often a multicomponent system with small amounts of impurities or the nature and the existence of the impurities is completely unknown.

Prince and Blanch (1990) have presented a coalescence rate model based on the film thinning theory. According to Prince and Blanch, the coalescence rate can be calculated from the bubble-bubble collision rate and coalescence efficiency.

$$\Omega_C(v_i, v_j) = \theta_{i,j}\lambda_{C,i,j} \tag{31}$$

Collisions between bubbles occur mainly by two mechanisms, by turbulent fluctuations of the liquid phase and by different rising velocities of bubbles of different size.

The turbulent collision rate can be expressed as

$$\theta_{i,j} = 0.089\pi N_i N_j (d_i + d_j)^2 \varepsilon^{1/3} (d_i^{2/3} + d_j^{2/3})^{1/2} \tag{32}$$

The buoyancy-driven collision rate is defined as

$$\theta_{i,j} = N_i N_j S_{i,j}(u_i - u_j) \tag{33}$$

$S_{i,j}$ is the cross-sectional area between the colliding bubbles defined as

$$S_{i,j} = \frac{\pi}{4}(d_i + d_j)^2 \tag{34}$$

In the film thinning model of Prince and Blanch (1990), a thin liquid film is left between the bubbles when the bubbles collide. This film drains from the original thickness to some critical thickness, where the film ruptures and coalescence occurs. Coalescence efficiency is assumed to be a function of the ratio of film drainage time to the time the bubbles remain in contact.

$$\lambda_{C,i,j} = \exp\left(-\frac{t_{i,j}}{\tau_{i,j}}\right) \tag{35}$$

where $t_{i,j}$ is the film thinning time required for film rupture and $\tau_{i,j}$ is the contact time of bubbles.

The contact time of the two bubbles can be estimated from

$$\tau_{i,j} = \frac{(0.5 d_{i,j})^{2/3}}{\varepsilon^{1/3}} \tag{36}$$

For pure liquids, neglecting the Hamaker force, which is significant only for very small film thickness prior to rupture, Prince and Blanch develop the following expression for film thinning time.

$$t_{i,j} = \left(\frac{(r_{i,j})^3 \rho_L}{16\sigma}\right)^{0.5} \ln\frac{h_0}{h_f} \tag{37}$$

where h_0 is the initial film thickness between colliding bubbles (1.0×10^{-4} m) and h_f is the final film thickness at film rupture (1.0×10^{-8} m).

$r_{i,j}$ is the equivalent radius for two different sized bubbles and may be expressed as

$$r_{i,j} = \left(\frac{1}{r_i} + \frac{1}{r_j} \right)^{-1} \tag{38}$$

The original film thinning time by Prince and Blanch (1990) does not include any parameters for the effect of the liquid composition. Therefore, the film thinning time was modified by Laari and Turunen (2003) to include an experimental coalescence parameter C.

$$t_{i,j} = C \left(\frac{(0.5 d_{i,j})^3 \rho_L}{16\sigma} \right)^{0.5} \ln \frac{h_0}{h_f} \tag{39}$$

In this thesis the coalescence efficiency is further modified by replacing the film thinning time in Equation (35) by a coalescence time. An estimate for the coalescence time can be obtained by parameter estimation using the experimentally obtained bubble size distributions in the column. The modified coalescence efficiency is presented by

$$\lambda_{i,j} = \exp\left(-\frac{t_C}{\tau_{i,j}} \right) \tag{40}$$

3.2 Bubble persistence time model

An alternative to the film-thinning model has been presented by Ghosh and Juvekar (2002) and Ghosh (2004). The model was developed for a case when a bubble (or drop) rests at a free liquid-gas interface. When the bubble hits the surface the adsorbate molecules are displaced in the outward direction and a high concentration of adsorbate is formed in the barrier ring. The model is based on the assumption that the bubble rests at the interface as a result of the repulsive force generated by a high concentration of adsorbate molecules on the opposite faces of the barrier ring. The repulsive force can be of double layer or steric/hydration force type. The repulsive force decays in time as the adsorbate is diffused from the barrier ring to the centre area where the adsorbate is initially depleted.

According to persistence time measurements the process is stochastic in nature. Instead of one single value for the persistence time, a distribution is obtained. The main reason for this is the inhomogeneity in the surface concentration on the barrier ring separating the bubble and the main liquid.

The cumulative persistence time probability is given by

$$F(\tau_R) = \frac{1}{2}\left[\operatorname{erf}\left\{\frac{1}{S_\Gamma\sqrt{2}}\left(\frac{P_\Gamma}{\left(1+\sum_{i=1}^{\infty} e^{-\kappa_i^2\tau_R}\right)}\right)\right\} + \operatorname{erf}\left(\frac{1}{S_\Gamma\sqrt{2}}\right)\right] \tag{41}$$

where λ_i are the roots of the Bessel function.

τ_R is the dimensionless persistence time, defined as $\tau_R = t/\bar{t}$ where $\bar{t}$ is the characteristic diffusion time given by

$$\bar{t} = \frac{R_b^2}{D_\Gamma} \tag{42}$$

D_Γ is the surface diffusivity of the adsorbate at the interface. For surfactants its value can be taken as 1×10^{-10} m^2/s and for amphiphiles as 2×10^{-10} m^2/s.

R_b is the radius of the barrier ring, which can be estimated from

$$R_b = 2r^2\sqrt{\frac{\Delta\rho g}{3\sigma}} \tag{43}$$

P_Γ is the dimensionless coalescence threshold, defined as

$$P_\Gamma = \frac{\Gamma_m}{\alpha\bar{\Gamma}_i} = \frac{r}{(w_b f_r \alpha)\bar{\Gamma}_i}\sqrt{\frac{\Delta\rho g\sigma}{3}} \tag{44}$$

S_Γ is the normalized standard deviation in surface excess, given by

$$S_{\Gamma} = \frac{\sigma_{\Gamma}}{\overline{\Gamma}_i} \tag{45}$$

S_{Γ} and P_{Γ} are parameters that can be estimated by fitting the cumulative rest time distribution of Equation (41) to the measured distribution.

3.3. Measurement of bubble persistence times

The method presented by Gosh and Juvekar (2002) and Ghosh (2004) was used to measure persistence times of different solutions, including de-ionized water, tap water, 0.1 kg/m^3 of isopropanol in de-ionized water, 0.2 % monopropylenegylycol in de-ionized water and solutions of 0.0025 dm^3/m^3 and 0.1 dm^3/m^3 of defoamer (Hercules™ BF 100) in tap water. The results are presented in paper V.

Measurements were carried out in a transparent chamber with a volume of 1 dm^3. A silicone plug or a teflon septum penetrating the column wall was used at the bottom of the vessel, which permitted direct injection of gas bubbles into the liquid. Each gas bubble was allowed to grow slowly at the tip of the needle before its release in order to achieve surface concentration equilibrium. Gas bubbles were released at the depth of 10 mm from the gas-liquid interface. The bubbles accelerated rapidly into their terminal velocity within a distance of a few millimeters.

The movement of the bubbles was followed using high-speed video camera with a maximum frame rate of 1000 1/s. The size of the bubble was measured after the bubble had been released from the tip of the needle. The bubble size was not controlled in the experiments and it ranged from 2 to 3 mm. The effect of the bubble size on the persistence time in this size range was found to be weak and the cumulative coalescence probabilities were calculated using all data points.

The measured persistence times range from 10 ms to 15 s depending on the solution. The observed coalescence was never instantaneous. When the bubble hit the free gas-liquid surface, the bubble and the liquid film between the bubble and the gas phase oscillated up and

down at least a couple of times before coalescence was observed. This fully support the observations made by Ghosh and Juvekar (2002).

The surface tension of the studied solutions was measured by Du Noüy ring method and the obtained values are shown in Table 2. Table 2 shows that the surface tension decreases only slightly and the changes in the coalescence behavior of the solutions cannot be explained by the decrease in the surface tension.

Table 2. Surface tension of the studied liquids.

Liquid	Surface tension, mN/m
De-ionized water	72
Tap water	72
0.1 kg/m^3 isopropanol in de-ionized water	71
0.2 % MPG* in de-ionized water	69
0.0025 dm^3/m^3 defoamer** in tap water	72
0.01 dm^3/m^3 defoamer** in tap water	72

*) monopropyleneglycol
**) Hercules™ BF 100 defoamer

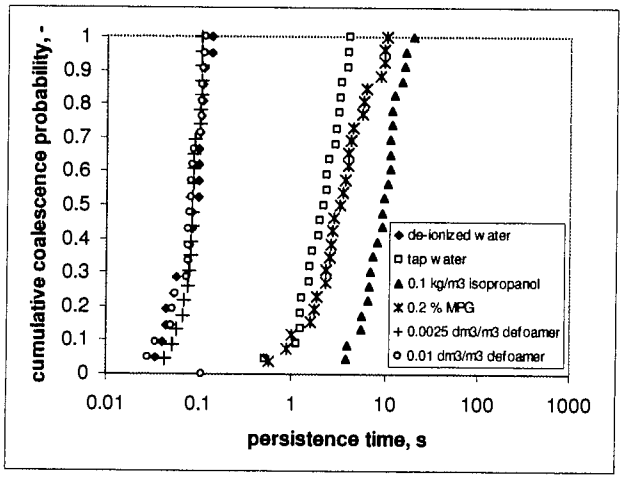

Figure 4. Measured cumulative coalescence probabilities for the studied solutions.

The parameters P_Γ and S_Γ in the persistence time probability model in Equation (41) were estimated by fitting the parameters to the measured cumulative probabilities. Surface diffusivity was assumed to be 1×10^{-10} m^2/s. The results are shown in Table 3. The results show that a good fit can be obtained in all cases with a high value for the coefficient of

determination (R^2). The identifiability of the parameters is good with a low relative standard error and low cross-correlation factor.

Table 3. Estimated persistence time model parameter values for the studied solutions and their relative standard error. ccf = cross-correlation factor.

	P_Γ	σ, %	S_Γ	σ, %	ccf. -	R^2, %
De-ionized water (DW)	2800	1.1	0.254	9.9	0.393	93.8
Tap water (TW)	562	0.6	0.252	4.1	0.180	98.6
0.2 % MPG* in DW	458	0.7	0.331	3.9	0.171	98.9
0.1 kg/m^3 isopropanol in DW	279	0.5	0.201	4.8	0.191	98.3
0.025 dm^3/m^3 of defoamer** in TW	2780	0.4	0.0954	8.6	0.187	95.3
0.1 dm^3/m^3 of defoamer** in TW	2860	0.8	0.157	9.4	0.288	94.7

*) monopropyleneglycol
**) Hercules™ BF 100

The persistence times obtained in this work can be compared to the coalescence times measured for two contacting bubbles by Chuang et al. (1984) and Ueyama et al. (1993). Chuang et al. (1984) studied the coalescence of two bubbles grown on two adjacent orifices. The coalescence time was measured using laser light and a light detector. The observed coalescence time for n-amyl alcohol solutions ranged from 20 ms to 200 ms for concentrations ranging from 10 to 75 ppm. The magnitude of the coalescence times observed by Chuang et al. is similar to that observed in this work. Very similar experimental system have been used by Ueyama et al. (1993) to measure the coalescence time of two bubbles formed at two nozzles using also a laser beam and a light detector. In their experimental system, however, a bubble formed at a movable nozzle was made to approach and contact the other bubble at a fixed nozzle. The observed coalescence time was found not to depend on the bubble approach velocity. The measured coalescence time for pure liquids is very low, around 0.3 ms, which indicates an almost instantaneous coalescence. For contaminated liquids the coalescence time typically ranges from 5 ms to 100 ms. Also in this case the magnitude of the measured coalescence times is similar to those observed in this work, except for the very low values obtained for pure liquids. These discrepancies could be caused by the differences in the shape of the film between the contacting bubbles and between the bubble and air in the persistence time measurements. The film between the contacting bubbles is planar, whereas it is curved in the persistence time experiments. Also, there are probably some differences in the hydrodynamics around the bubble in the two cases.

4. Estimation of coalescence parameters from bubble column measurements

4.1 Population balance model for bubble column

The changes in the bubble size distribution can be expressed by means of population balance equations (PBEs). The population balance equation for bubbles in a flow system may be expressed in a general form in one spatial dimension (Colella et al., 1999; Fleischer, Becker and Eigenberger, 1996; Lehr and Mewes, 2001)

$$\begin{aligned}&\frac{\partial}{\partial t}n(t,v,z)+\frac{\partial}{\partial z}\left[n(t,v,z)u_b(v,z)\right]+\frac{\partial}{\partial v}\left[n(t,v,z)\frac{\partial}{\partial t}v(v,z)\right]\\&=\frac{\partial}{\partial t}\left[E_z(v,z)\frac{\partial}{\partial z}f(t,v,z)\right]+B(t,v,z)+C(t,v,z)\end{aligned} \tag{46}$$

The meaning of the terms from left to right is:

1. variation in time
2. variation due to bubble transport
3. variation due to mass transfer or expansion caused by change in pressure
4. bubble dispersion term
5. source term due to breakage
6. source term due to coalescence

For a bubble column operating in homogeneous flow regime at steady state, the general population balance equation can be simplified by neglecting the variation in time (term 1), variation due to mass transfer (term 3) and variation due to dispersion (term 4). Variation due to expansion can be neglected for short columns. For large columns this term can be neglected by using bubble mass as the internal coordinate instead of bubble volume. The dispersion term may be neglected for low gas superficial velocities. For higher gas superficial velocities with churn-turbulent gas-liquid flow the dispersion term becomes important. An additional problem then is that no data about bubble dispersion coefficients is available that could be implemented in the model.

The source terms for bubble breakage and coalescence can be expressed in a more detailed form (Ramkrishna, 2000; Kumar and Ramkrishna, 1996)

$$B(v,z) = B_B - D_B = \int_v^\infty \beta(v,v')\Omega_B(v')n(v',z)dv' - \int_0^\infty n(v,z)n(v',z)\Omega_C(v,v')dv' \tag{47}$$

$$C(v,z) = B_C - D_C = \frac{1}{2}\int_0^v n(v-v',z)n(v',z)\Omega_C(v-v',v)dv' - \int_0^\infty n(v,z)n(v',z)\Omega_C(v,v')dv' \tag{48}$$

where B_B is the birth term due to breakage, D_B is the death term due to breakage, B_C is the birth term due to coalescence and D_C is the death term due to coalescence.

The continuous population balance equation for flowing bubbles in a bubble column at steady state undergoing breakage and coalescence is then

$$u_b\frac{\partial n(v,z)}{\partial z} = \frac{1}{2}\int_0^v n(v-v',z)n(v',z)\Omega_C(v-v',v')dv' - \Omega_B(v)n(v,z) - \int_0^\infty n(v,z)n(v',z)\Omega_C(v,v')dv' + \int_v^\infty \beta(v,v')\Omega_B(v')n(v',z)dv' \tag{49}$$

where u_b is the velocity of bubble with respect to the column wall.

The actual bubble velocity in the column depends on bubble size and radial position in the column. The bubble velocity is highest in the column centre and lowest at the column wall. Bubble velocity also depends on the presence of other bubbles (bubble swarm velocity). The exact bubble velocity can only be estimated by solving the complete multiphase hydrodynamics by using computational fluid dynamics.

Additional approximations to Equation (49) were made by neglecting the radial variation of bubble velocity and assuming that each bubble rises with a velocity equal to the terminal rising velocity. In practice, this is equal to the assumption of a stagnant liquid phase.

The terminal rising velocity was calculated using the correlation presented by Rodrigue (2001)

$$V_N = \frac{s_1 F^{s_2}}{1 + s_3 F^{s_4}} \tag{50}$$

where the parameters s_1, s_2, s_3 and s_4 have values

$s_1 = 1/12$, $s_2 = 1$, $s_3 = 49/1000$, $s_4 = 3/4$.

The flow number F is defined as

$$F = Eö\left(\frac{Re}{Ca}\right)^{2/3} = g\left(\frac{d_b^8 \rho_L^5}{\sigma \mu_L^4}\right)^{1/3} \tag{51}$$

and the velocity number V_N as

$$V_N = \left(Re^2 Ca\right)^{1/3} = u_b\left(\frac{d_b^2 \rho_L^2}{\sigma \mu_L}\right)^{1/3} \tag{52}$$

Ca is the capillary number defined as

$$Ca = \frac{\mu_L u_b}{\sigma} \tag{53}$$

4.1.1 Solution of population balances

Analytical solution of the population balance equation (49) or its transient counterpart in a well-mixed system

$$\begin{aligned}\frac{\partial n(v,t)}{\partial t} = \frac{1}{2}\int_0^v n(v-v',t)n(v',t)\Omega_C(v-v',v')dv' - \Omega_B(v)n(v,t) \\ - \int_0^\infty n(v,t)n(v',t)\Omega_C(v,v')dv' + \int_v^\infty \beta(v,v')\Omega_B(v')n(v',t)dv'\end{aligned} \tag{54}$$

is only possible for some limited cases.

Several numerical methods have been proposed to solve the continuous population balance equation. These include, according to Ramkrishna (2000), the method of weighted residuals, method of moments, orthogonal collocation, and collocation on finite elements.
The method of discretization has been proposed by Kumar and Ramkrishna (1996) as a computationally efficient alternative. In the method of discretization the particle population in the size range $\{v_i, v_{i+1}\}$ is assumed to be concentrated to one size point x_i, the so called representative size (or grid/pivot point).

$$n(v,t) = \sum_{j=1}^{M} N_j \delta_K (v - x_j) \tag{55}$$

where M is the number of discretization points and δ is the Kronecker delta function.

By introducing Equation (55) into the continuous PBE, the continuous PBE can be transformed into a discretized form. Kumar and Ramkrishna (1996) have derived the following discretized PBE.

$$\begin{aligned} \frac{dN_i(t)}{dt} = & \sum_{\substack{j,k \\ x_{i-1} \le (x_j + x_k) \le x_{i+1}}}^{j \ge k} \left(1 - \frac{1}{2}\delta_{j,k}\right) \eta \Omega_{C,j,k} N_j(t) N_k(t) - N_i(t) \sum_{k=1}^{M} \Omega_{B,i,k} N_k \\ & + \sum_{k=i}^{M} n_{i,k} \Omega_{B,k} N_k(t) - \Omega_{B,i} N_i(t) \end{aligned} \tag{56}$$

One should pay attention to the fact that after the discretization only the 0th moment of the continuous distribution (number of bubbles) is conserved. To preserve another moment of the distribution requires the implementation of some carefully chosen correction terms for the coalescence and breakage birth terms. Usually preservation of the 0th and 3rd moments of the distribution (numbers and volume (or mass) of bubbles) is desired. Equation (56) includes one correction term (η) in the birth by coalescence term and one correction term in the birth by breakage term ($n_{i,k}$).

According to Kumar and Ramkrishna (1996), the general form of the correction term in the coalescence birth term is

$$\eta = \begin{cases} \dfrac{v^{\zeta} x_{i+1}^{\nu} - v^{\nu} x_{i+1}^{\zeta}}{x_i^{\zeta} x_{i+1}^{\nu} - x_i^{\nu} x_{i+1}^{\zeta}}, & x_i \le v \le x_{i+1} \\ \dfrac{v^{\zeta} x_{i-1}^{\nu} - v^{\nu} x_{i-1}^{\zeta}}{x_i^{\zeta} x_{i-1}^{\nu} - x_i^{\nu} x_{i-1}^{\zeta}}, & x_{i-1} \le v \le x_i \end{cases} \tag{57}$$

η is given by the formula

$$\eta = \begin{cases} \dfrac{x_{i+1} - v}{x_{i+1} - x_i}, & x_i \le v \le x_{i+1} \\ \dfrac{x_{i-1} - v}{x_{i-1} - x_i}, & x_{i-1} \le v \le x_i \end{cases} \tag{58}$$

for the conservation of numbers and mass.

The correction term for the birth term by breakage is

$$n_{i,k} = \frac{B_{i,k}^{(\xi)} x_{i+1}^{\nu} - B_{i,k}^{(\nu)} x_{i+1}^{\zeta}}{x_i^{\zeta} x_{i+1}^{\nu} - x_i^{\nu} x_{i+1}^{\zeta}} + \frac{B_{i-1,k}^{(\xi)} x_{i-1}^{\nu} - B_{i-1,k}^{(\nu)} x_{i-1}^{\zeta}}{x_i^{\zeta} x_{i-1}^{\nu} - x_i^{\nu} x_{i-1}^{\zeta}} \tag{59}$$

where $B_{i,k}^{(\xi)}$ is given as

$$B_{i,k}^{(\xi)} = \int_{x_i}^{x_{i+1}} v^{\xi} \beta(v, x_k) dv \tag{60}$$

The exact preservation of numbers and mass is achieved by setting $\zeta = 0, \nu = 1$.

$$n_{i,k} = \int_{x_i}^{x_{i+1}} \frac{x_{i+1} - v}{x_{i+1} - x_i} \beta(v, x_k) dv + \int_{x_{i-1}}^{x_i} \frac{v - x_{i-1}}{x_i - x_{i-1}} \beta(v, x_k) dv \tag{61}$$

The method by Kumar and Ramkrishna (1996) is suitable for any arbitrary discretization. An additional benefit of this method is that it can be set to preserve any two moments of the distribution, for example, numbers and interfacial area, if that is preferred.

Another useful discretization method has been proposed by Hagesaether et al. (2002). In this method, the discretization of bubble size is based on a geometrical scheme where the next largest size class has a mass (or volume) of two times the mass of the previous class.

$$m_{i+1} = 2m_i \tag{62}$$

As shown by Hagesaether et al. (2002), the coalescence and breakage birth and death terms can be formulated in such a way that both numbers and mass are conserved. Hence, no other correction factors are needed.

According to Hagesaether et al. (2002) the break-up death rate is

$$D_B(i) = \sum_{k=1}^{i-1} \Omega_B(m_i, m_k), \text{ for } i = 2...N_C \tag{63}$$

and the break-up birth rate

$$B_B(i) = \sum_{k=i+1, i\neq N_C}^{N_C} \Omega_B(m_k, m_i) + \sum_{k=1, i\neq N_C}^{i} x_{i+1,k}\, \Omega_B(m_{i+1}, m_k) + \sum_{k=1}^{i-1} (1 - x_{i,k}) \Omega_B(m_i, m_k), \tag{64}$$

for $i = 1...N_C$

The coalescence death rate is

$$D_C(i) = \sum_{j=1}^{N_C-1} \Omega_C(m_i, m_j) + \Omega_C(m_i, m_i), \text{ for } i = 1...N_C \tag{65}$$

and the coalescence birth rate

$$B_C(i) = \sum_{j=1, i\neq N_C}^{i-1} x_{i,j} \Omega_C(m_i, m_j) + \sum_{j=1}^{i-1} (1 - x_{i-1,j}) \Omega_C(m_{i-1}, m_j), \text{ for } i = 2...N_C \tag{66}$$

The terms $x_{i,k}$ and $x_{i,j}$ in the birth terms of breakage and coalescence are defined as

$$x_{i,k} = 2^{1+k-i}, \; k < i \tag{67}$$

$$x_{i,j} = 1 - 2^{j-i}, \; i \geq j \tag{68}$$

The population balance equation (49) is transformed by the discretization method into a set of ordinary differential equations the number of which equals the number of bubble classes used for the discretization.

$$u_b \frac{dN_i(z)}{dz} = B_C + B_B - D_C - D_B \tag{69}$$

The differential equations can be solved numerically by integrating the equations starting form the initial value at the bottom of the reactor.

4.2 Parameter estimation and parameter identifiability

The coalescence and breakage parameters can be estimated by comparing the measured and calculated bubble size distributions or mean bubble sizes. In this work the Sauter mean bubble size was chosen for the comparison. This was done because all the measured distributions were found to be monomodal and convergence could be obtained more easily by using mean sizes instead of complete distributions.

A good parameter fit can be characterized as having a good coefficient of determination (R^2-value), low standard error for the estimated parameters and good parameter identifiability. Even though the estimated parameters would predict the measured values well with a good regression coefficient, the estimated parameters can have large standard errors and be substantially intercorrelated. In practical terms this means that a large number of parameter combinations give equally good fit. In this case, the identifiability and reliability of the estimated parameters is poor. Parameter identifiability can be studied by drawing contour plots for constant R^2 values, or values of objective function, with varying intervals between the parameters that are most intercorrelated.

4.2.1 Cylindrical bubble column

Bubble size distributions were measured photometrically in a cylindrical bubble column with a diameter of 0.078 m and height of 4.6 m by video recording the bubbly flow at several

height positions, which were 0 m, 0.35 m, 0.9 m, 1.65 m and 2.4 m. Due to the limitations of the technique only bubbles at the column wall can be detected. A set of 100 bubbles was calculated manually at each height position. Gas superficial velocities were 1, 2 and 6 cm/s. Eight different gas spargers were used in the experiments. Their characteristics are shown in Table 4.

The measured Sauter mean bubble sizes are shown in Table 5 and in Figures 5 and 6. Sauter mean bubble size is defined as

$$d_{32} = \frac{\sum_{i=1}^{N} n_i d_i^3}{\sum_{i=1}^{N} n_i d_i^2} \tag{70}$$

Table 4. Properties of the gas spargers.

Name	Sparger type	Number of holes	Diameter of holes, mm	Free area of holes, %	Distance between holes, mm
Sp1	Tube	2000	0.07	-	-
Sp2	Perforated plate	11	0.5	0.045	17.23
Sp3	Perforated plate	22	0.5	0.090	12.18
Sp4	Perforated plate	66	0.5	0.27	7.03
Sp5	Perforated plate	6	1	0.090	23.32
Sp6	Perforated plate	382	0.12	0.090	2.92
Sp7	Porous plate	-	0.04	-	-
Sp8	Perforated plate	1414	0.12	0.060	3.80

Table 5. Average gas holdup and Sauter mean bubble size in a cylindrical bubble column with a diameter of 0.078 m and height 4.58 m. Temperature is 45 °C. Superficial gas velocity is measured at 20 °C and normal pressure. Physical properties of the process solution at 45 °C are: Density 1389 kg/m3, dynamic viscosity 2.5 mPa s and surface tension 57-69 mN/m.

solution	sparger	U_G, m/s	$\bar{\varepsilon}_G$, %	Sauter mean bubble size, mm				
				Z=0 m	Z=0.35 m	Z=0.9 m	Z=1.65 m	Z=2.4 m
Tap water	Sp 1	0.01	3.6	2.45	3.56	3.98	4.53	5.31
Tap water	Sp 1	0.02	6.8	2.22	4.61	5.13	5.45	5.75
Tap water	Sp 1	0.06	14.8	3.14	6.20	6.00	5.10	5.93
Tap water	Sp 3	0.01	3.3	4.13	4.54	4.37	5.22	5.42
Tap water	Sp 3	0.02	6.8	4.60	5.04	5.30	5.34	6.84
Tap water	Sp 3	0.06	15.4	5.21	5.99	6.22	6.53	6.65
Tap water	Sp 6	0.01	4.0	1.50	3.20	4.01	5.23	5.30
Tap water	Sp 6	0.02	7.4	1.63	4.36	4.81	5.51	6.18
Tap water	Sp 6	0.06	15.7	2.31	5.87	5.84	5.21	5.32
Tap water	Sp 7	0.01	3.2	1.53	3.96	5.66	5.91	6.50
Tap water	Sp 7	0.02	6.4	1.40	4.31	5.61	5.62	5.41
Tap water	Sp 7	0.06	14.4	2.38	4.60	6.18	5.83	5.05
Process solution	Sp 2	0.01	3.3	4.46	4.83	4.95	4.99	5.36
Process solution	Sp 2	0.02	6.8	5.41	4.87	4.68	5.50	5.29
Process solution	Sp 3	0.01	3.6	4.28	4.30	4.70	4.53	5.07
Process solution	Sp 3	0.02	8.0	4.78	4.79	4.72	4.81	5.08
Process solution	Sp 5	0.01	2.9	6.95	6.55	5.45	4.92	4.77
Process solution	Sp 5	0.02	6.1	7.93	4.59	4.23	4.19	4.62
Process solution	Sp 6	0.01	4.3	1.65	2.18	2.34	2.21	2.30
Process solution	Sp 6	0.02	10.1	1.87	2.39	2.32	2.48	2.77

Table 5 shows that the coalescence rate with tap water is faster than the breakage rate and the Sauter mean bubble size increases with all spargers and gas flow rates and approaches a stable bubble size.

For process solution the coalescence rate is slow and bubble size increases only slightly in some cases. In some cases the initial bubble size at the bottom of the column is larger than the maximum stable bubble size and the Sauter mean bubble size decreases as the bubbles move upwards in the column.

The size distributions and the Sauter mean sizes were calculated by solving the differential equations formed by the population balances of Equation (69).

The estimated coalescence and breakage parameters are shown in Table 6 and the measured and calculated Sauter mean bubble sizes in Figures 5 and 6. Two breakage models were tested, the model by Prince and Blanch (1990), Equation (9), and the model by Colella et al., Equation (14). Coalescence efficiency was calculated by using the coalescence model of Prince and Blanch, Equation (39), with one experimental parameter C .

The estimated values for the breakage parameter, the critical Weber number, 1.8 for tap water and 1.7 for the process solution, are relatively close to the value of 2.3 given by Prince and Blanch (1990) for pure water

Table 6. Estimated coalescence and break-up parameters for tap water and process solution in a bubble column. ccf = cross-correlation factor between coalescence and breakage parameters.

Case	Liquid	Coalescence model	Break-up model	Coalescence parameter	Break-up parameter	R^2, %	ccf, -
Case 1	Tap water	Prince and Blanch (1990)	Prince and Blanch (1990)	C = 3.93	We_c = 1.83	96.8	0.44
Case 2	Tap water	Prince and Blanch (1990)	Colella et al. (1999)	C = 3.47	k_w = 9560	97.0	-0.89
Case 3	Process solution	Prince and Blanch (1990)	Prince and Blanch (1990)	C = 9.51	We_c = 1.67	95.6	0.05
Case 4	Process solution	Prince and Blanch (1990)	Colella et al. (1999)	C = 3.34	k_w = 21 700	93.0	-0.85

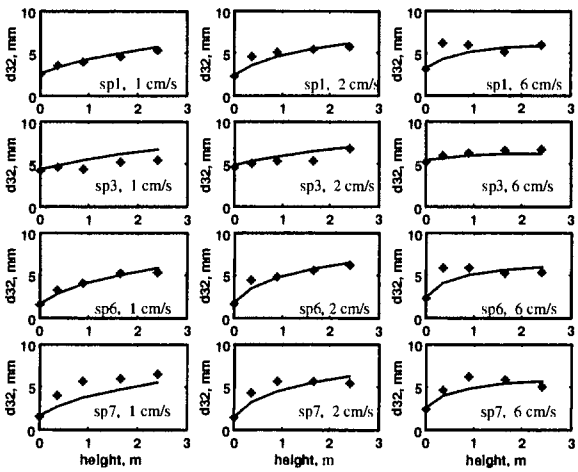

Figure 5. Measured and predicted profiles of Sauter mean bubble size with different gas spargers and different gas superficial velocities. Case 1: Tap water, coalescence model of Prince and Blanch, break-up model of Prince and Blanch.

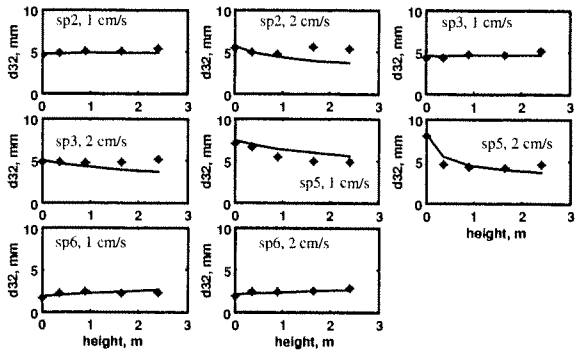

Figure 6. Measured and predicted profiles of Sauter mean bubble size with different gas spargers and gas superficial velocities.
Case 3: Process solution, coalescence model of Prince and Blanch, break-up model of Prince and Blanch.

Parameter identifiability was studied by drawing LSQ –profiles and contour plots for the estimated coalescence and breakage parameters. These are shown in Figures 7 - 10.

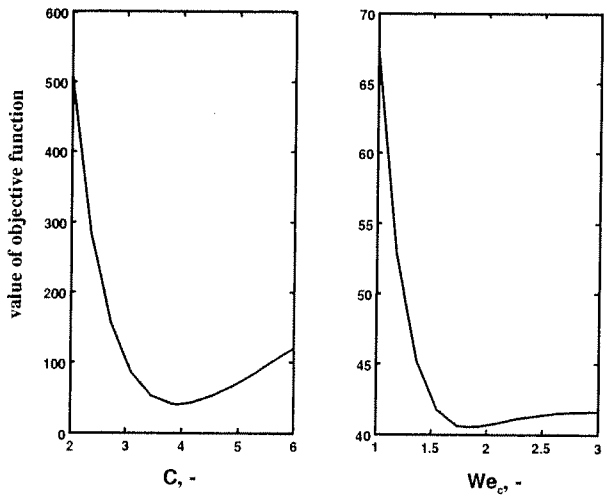

Figure 7. LSQ profiles for the parameters of case 1 (Tap water, coalescence model of Prince and Blanch, break-up model of Prince and Blanch).

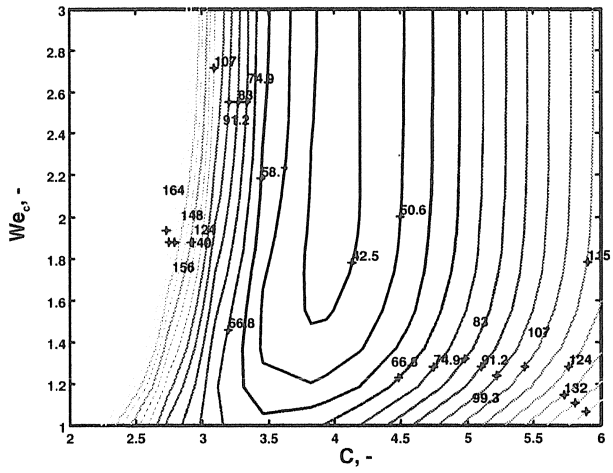

Figure 8. Contour plot for the parameters of case 1 (Tap water, coalescence model of Prince and Blanch, break-up model of Prince and Blanch).

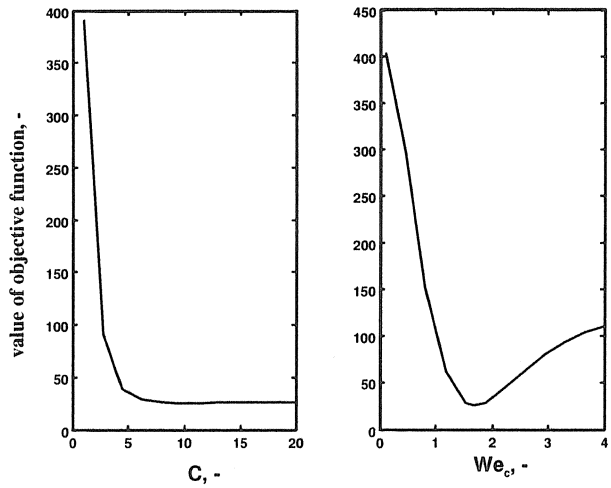

Figure 9. LSQ profiles for the parameters of case 3 (process solution, coalescence model of Prince and Blanch, break-up model of Prince and Blanch).

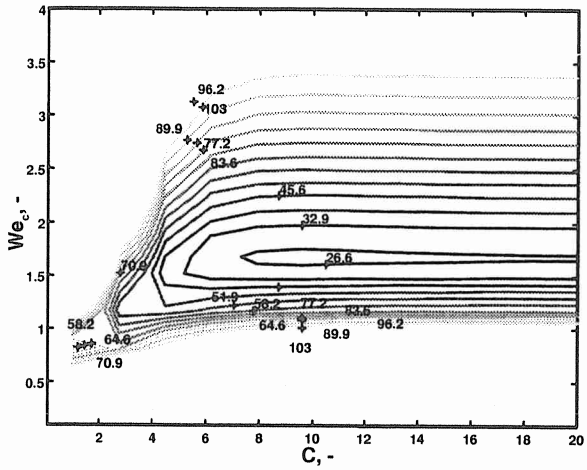

Figure 10. Contour plot for the parameters of case 3 (process solution, coalescence model of Prince and Blanch, break-up model of Prince and Blanch).

The parameter identifiability study shows that for tap water the coalescence parameter is well identified, a clearly distinguishable optimum can be seen with respect to the parameter value (see Figure 7, on the left). For tap water the breakage parameter is not that well-identified, only a weak optimum can be seen in Figure 7 (on the right). The same phenomenon can be observed in the contour plot in Figure 8. The reason for the poor identifiability of the breakage parameter for tap water is that all the experiments were done in conditions in which the bubble size increases and bubble coalescence dominated over bubble breakage.

For the process solutions the situation is the opposite. Bubble breakage dominates and the mean bubble size increases only slightly in some cases. The parameter identifiability study shows that the bubble breakage parameter is well identified, as shown in Figure 9 on the right. The coalescence parameter, however, is poorly identified and the only thing that can be said about the coalescence parameter is that its value is over 5 (see Figure 9 , on the left).

The parameter identifiability study clearly demonstrates the fact that to simultaneously obtain reliable coalescence and breakage parameters the measurements have to be done so that at least in some cases a clearly distinguishable increase and decrease in the bubble size can be observed.

4.2.2 Rectangular bubble column

Bubble size distributions were measured at five different height positions, which were 0 m, 0.25 m, 0.5 m, 1.0 m and 1.5 m, in a rectangular bubble column with a width of 0.15 m, depth of 0.03 m and height of 1.5 m. A LED light panel was used at the back of the column to illuminate bubbles rising in the liquid solution. A photographic method was used to obtain bubble size distributions at each height position by video recording the bubbly flow with a Canon MX1 video camera using progressive frame mode, a shutter speed of 1/500 s and aperture of f8 for two minutes. Frames were captured from the video recording and saved as bitmap images.

ImageJ software was used to detect bubbles automatically and to analyze their size and shape. Several shape describing parameters, presented in Table 8, were calculated for each bubble. Even though the gas holdup was relatively low, some bubbles in the image were usually overlapping. Based on the shape describing parameters shown in Table 8, some bubbles were removed from the data and only those bubbles fulfilling the shape describing parameter criteria were accepted. The shape descriptor limit values were roughly obtained by comparing bubble shapes visually in some frames.

Table 7. Average gas holdup and Sauter mean diameter in a rectangular bubble column. Temperature 20 °C, normal pressure.

solution	U_G, m/s	$\bar{\varepsilon}_G$, %	Sauter mean bubble size, mm				
			Z = 0 m	Z=0.35 m	Z=0.9 m	Z=1.65 m	Z=2.4 m
Tap water (TW)	0.0037	2.26	2.29	3.05	3.30	3.60	3.50
Tap water (TW)	0.0074	4.47	2.76	3.51	3.81	4.01	4.00
De-ionized water (DW)	0.0037	2.34	2.44	3.04	3.36	3.56	3.86
De-ionized water (DW)	0.0074	3.84	3.09	3.71	4.01	4.11	4.24
0.1 kg/m3 isopropanol in DW	0.0037	2.09	2.83	2.96	2.89	2.93	3.15
0.1 kg/m3 isopropanol in DW	0.0072	4.39	2.92	3.02	2.77	2.87	3.18
0.2 % MPG* in DW	0.0037	2.35	1.21	1.26	1.25	1.16	1.33
0.0025 dm3/m3 defoamer** in TW	0.0019	1.02	2.19	2.48	2.67	3.02	3.36
0.0025 dm3/m3 defoamer** in TW	0.0037	2.04	2.59	3.04	3.24	3.52	3.69
0.01 dm3/m3 defoamer** in TW	0.0019	0.98	2.22	2.88	3.38	3.61	4.15
0.01 dm3/m3 defoamer** in TW	0.0037	1.85	2.81	3.56	3.99	4.39	5.05
0.03 dm3/m3 defoamer** in TW	0.0019	0.86	2.28	2.86	3.38	3.99	4.33
0.03 dm3/m3 defoamer** in TW	0.0037	1.73	2.74	3.52	4.48	5.33	6.00

*) monopropyleneglycol
**) Hercules™ BF 100 defoamer

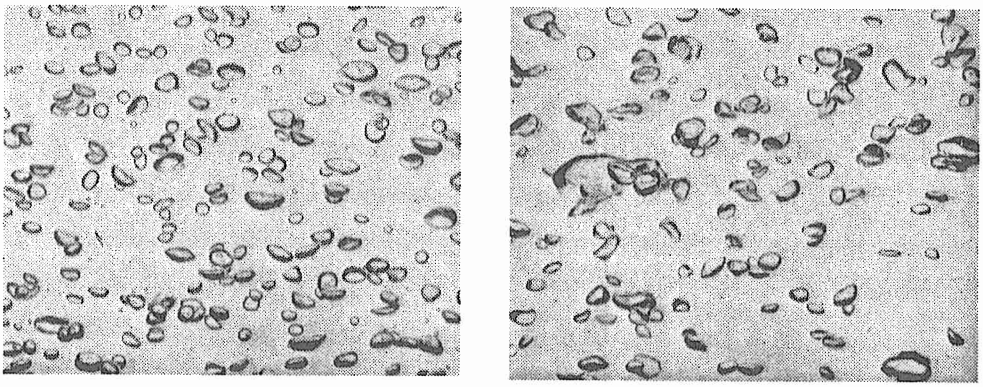

Figure 11. Photograph of bubbly flow in 0.1 kg/m^3 isopropanol in de-ionized water (on the left) and 0.01 dm^3/m^3 of Hercules BF 100 defoamer in tap water (on the right) at the height of 1.5 m.

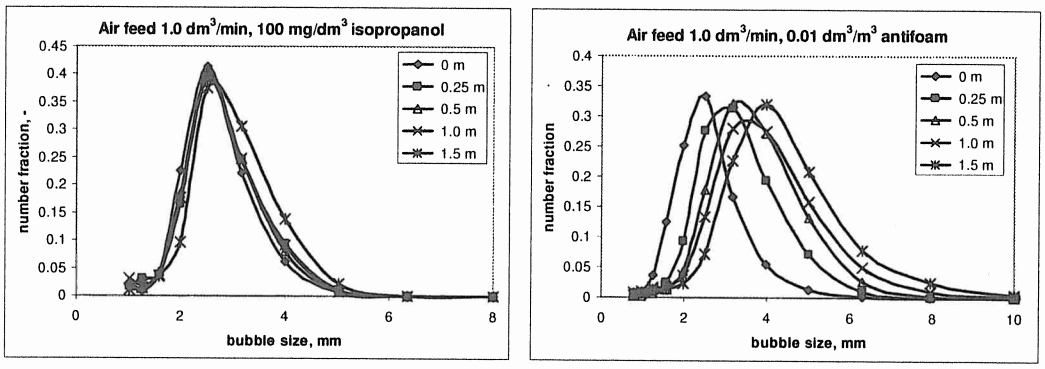

Figure 12. Measured bubble size distributions in the rectangular bubble column for a slowly coalescing solution (on the left) and for a rapidly coalescing solution (on the right).

Table 8. Rejection limit values for the shape describing parameters.

Shape parameter	Definition	Rejection limit value
Form factor	$4\,\pi$ area/(perimeter)$^{0.5}$	< 0.7
Roundness	4 area/ π (major axis)$^{0.5}$	< 0.7
Compactness	((4/π) area)$^{0.5}$/major axis	< 0.6
Aspect ratio	major axis/minor axis	> 3.0
Solidity	area/ convex area	< 0.9
Convexity	convex perimeter/perimeter	< 0.95

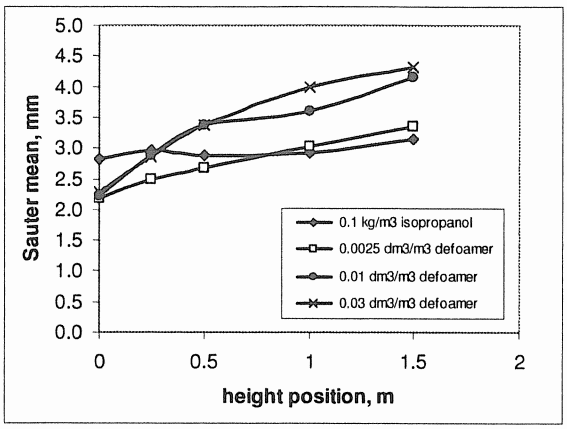

Figure 13. Measured profiles of Sauter mean bubble size for superficial gas velocity 0.19 cm/s.

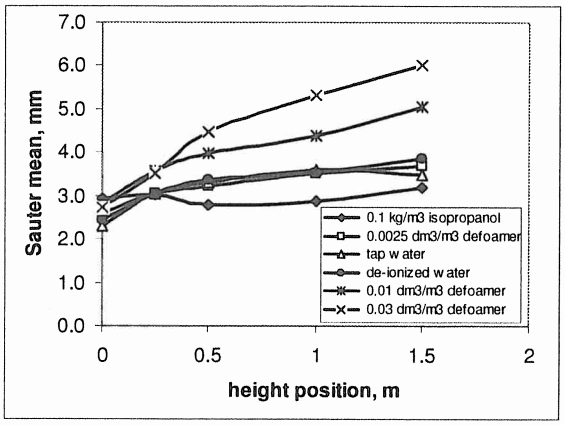

Figure 14. Measured profiles of Sauter mean bubble size for superficial gas velocity 0.37 cm/s.

The coalescence parameter for the film thinning model and the coalescence time in equations (39) and (40) were estimated by comparing the measured and calculated Sauter mean bubble sizes. In all cases a good agreement between the measured and calculated values was obtained, as can be seen from Figure 15. The coefficient of determination (R^2) is over 96 % for all studied solutions, except the case of 0.2 % MPG in de-ionized water. The estimated parameters are shown in Table 9.

Table 9. Estimated coalescence parameter for film thinning model and coalescence time.

Liquid	Gas superficial velocity 0.19 cm/s				Gas superficial velocity 0.37 cm/s			
	Film thinning model		Coalescence time		Film thinning model		Coalescence time	
	C, -	R^2, %	t_C, s	R^2, %	C, -	R^2, %	t_C, s	R^2, %
Tap water (TW)	-	-	-	-	7.40	96.7	0.0941	95.8
De-ionized water (DW)	6.12	97.3	0.0726	97.2	6.42	98.0	0.0951	97.9
0.1 kg/m^3 isopropanol in DW	-	-	-	-	17.5	96.5	0.236	96.5
0.2 % MPG in DW	-	-	-	-	47.2	55.1	0.166	55.1
0.0025 dm^3/m^3 defoamer in TW	7.47	97.2	0.0860	97.2	7.71	97.7	0.110	97.5
0.01 dm^3/m^3 defoamer in TW	4.33	97.6	0.0612	97.2	4.67	98.6	0.0878	98.3

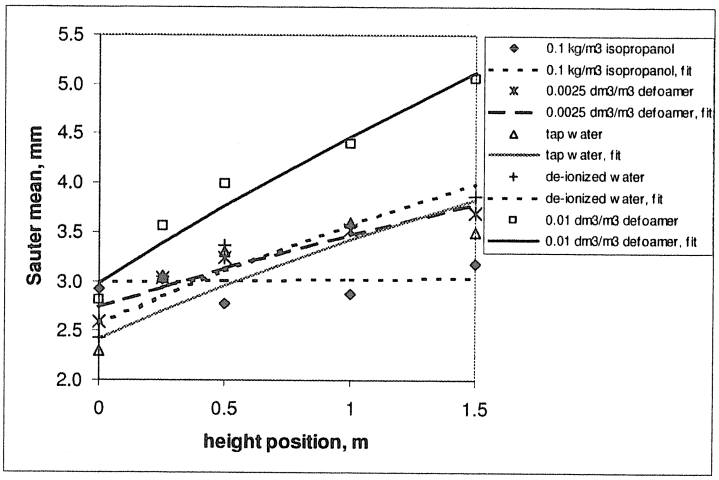

Figure 15. Measured and estimated profiles of Sauter mean bubble size in the column. Gas superficial velocity 0.37 cm/s.

A comparison of the measured persistence times and the estimated coalescence times is shown in Figure 16. For rapidly coalescing liquids with short persistence times the measured persistence times and the estimated coalescence times are in good agreement. This suggests that for rapidly coalescing liquids the film-thinning time can be replaced directly with the persistence time. However, for slowly coalescing liquids the estimated coalescence times are much shorter than the measured persistence times. The reason for this is that because the persistence time for the slowly coalescing liquids is at least an order of magnitude higher than for the coalescing liquids, the coalescence efficiency calculated from Equation (40) decreases drastically. There might be several reasons for this discrepancy. First of all, the contact time of bubbles in Equation (36) is an order of magnitude estimation of the actual contact time.

There is no accurate information available about the contact times of bubbles in bubbly flows. Also, the level of energy dissipation is probably overestimated, affecting the contact time and the turbulent collision rate of bubbles. Furthermore, it is not clear whether the bubble-bubble collision rate mechanism, including turbulent, rising velocity difference induced and shear induced collision rates, resembles the real bubble-bubble interaction. For example, the wake effect where a bubble is entrapped in the wake of the leading bubble is not included in the model. Nevertheless, Figure 16 gives a simple correlation between the measured persistence times and the coalescence time and it can be used to estimate the coalescence efficiency in a population balance model.

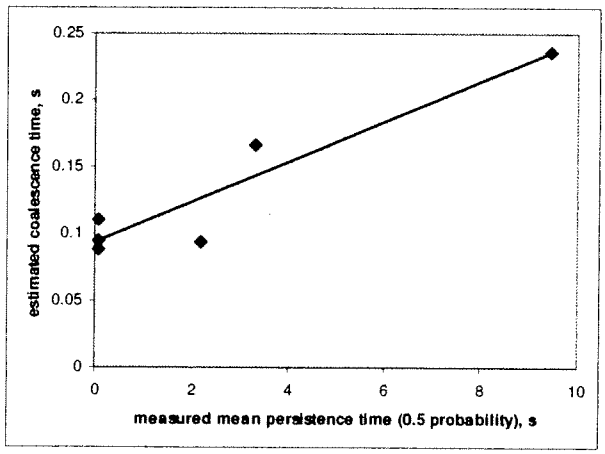

Figure 16. Comparison of the measured persistence times and the estimated coalescence times. Gas superficial velocity 0.37 cm/s.

5. Gas-liquid mass transfer

5.1 Liquid-side mass transfer coefficient

Several empirical correlations have been proposed to estimate the liquid mass transfer coefficient in bubbly flow, for example, Calderbank and Moo-Young (1961), Hughmark (1967), Akita and Yoshida (1974) and Oels et al. (1978). In these correlations mass transfer coefficient depends on average values of bubble size and gas velocity.

The accuracy of calculation of mass transfer in multiphase CFD would benefit a great deal if the liquid side mass transfer coefficient could be evaluated from local conditions using local particle size, local slip velocity between the particle and liquid and local turbulent intensity.

Theoretical models that can be applied for this purpose have been presented by Alves, Maia and Vasconcelos (2004) for a gas-liquid mixed tank based on slip velocity, by Kawase, Halard and Moo-Young (1987) for a bubble column, and by Garchia-Ochoa and Gomez (2004) and Linek et al. (2004) for a gas-liquid mixed tank based on turbulence energy dissipation rates.

All these models are based on Higbie's penetration theory

$$k_L = 2\sqrt{\frac{D_L}{\pi t_e}} \tag{71}$$

where t_e is an exposure time for mass transfer

The exposure time can be estimated either based on bubble and liquid slip velocity or on turbulence intensity.

For a fully mobile interface the exposure time can be estimated to be equal to the time it takes for the bubble to travel a length equal to its diameter.

$$k_L = \frac{2}{\sqrt{\pi}}\sqrt{D_L \frac{u_s}{d_b}} \tag{72}$$

For a rigid interface, mass transfer can be estimated from Frössling's theoretical equation for laminar flow.

$$k_L = c\sqrt{\frac{u_s}{d_b}} D^{2/3} \nu^{-1/6} \tag{73}$$

where the coefficient $c \approx 0.6$ according to Alves et al.

In practice, the surface mobility lies between fully mobile and rigid surfaces and the mass transfer coefficient is somewhere between the ones predicted by Equations (72) and (73). The mass transfer coefficient calculated for a mobile surface from Equation (72) is five times as high as for a rigid surface calculated from Equation (73).

For turbulent flow the exposure time in Equation (71) can be also estimated using Kolmogoroff's theory of isotropic turbulence. The gas-liquid surface is continuously bombarded by turbulent eddies with a scale smaller than the bubble size.

According to Kolmogoroff's theory, eddy length is

$$\eta = \left(\frac{\nu^3}{\varepsilon}\right)^{1/4} \tag{74}$$

And the fluctuation velocity

$$u = (\nu\varepsilon)^{1/4} \tag{75}$$

Taking the exposure time to be equal to eddy length divided by fluctuation velocity and inserting exposure time into Equation (71) gives

$$k_L = \frac{2}{\sqrt{\pi}}\sqrt{D_L}\left(\frac{\varepsilon\rho}{\mu}\right)^{1/4} \tag{76}$$

The experimentally obtained coefficients for Equation (76) ranging from 0.3 up to 0.6 are significantly lower that the theoretical value $2/\sqrt{\pi}$ (Linek et al., 2004). A possible reason for this discrepancy could be the difficulties involved in the estimation of turbulence energy dissipation rates in the dispersion.

It seems reasonable to assume that in turbulent gas-liquid flow both the surface renewal mechanisms, by slip velocity and turbulence, should be included in the mass transfer model. This can be done by assuming that both surface renewal mechanisms take place simultaneously and that the surface renewal rates are additive.

For a fully mobile interface one obtains

$$k_L = \frac{2}{\sqrt{\pi}}\sqrt{\frac{D_L}{t_e}} = \frac{2}{\sqrt{\pi}}\sqrt{D_L R} = \frac{2}{\sqrt{\pi}}\sqrt{D_L\left(\frac{u_s}{d_b} + \left(\frac{\rho\varepsilon}{\mu}\right)^{1/2}\right)} \tag{77}$$

and for rigid particles

$$k_L = c\frac{D^{2/3}}{\nu^{1/6}}\sqrt{\frac{u_s}{d_b} + \left(\frac{\rho\varepsilon}{\mu}\right)^{1/2}} \tag{78}$$

The proposed model for gas-liquid mass transfer in bubbly flows above is new and it should be verified by measurements in different conditions. This requires the development of experimental techniques for the measurement of local slip velocities and turbulent intensities.

5.2 Turbulent energy dissipation rate

The turbulent energy dissipation rate is an important parameter in gas-liquid bubbly flow that affects mass transfer, bubble coalescence and bubble breakage rates. The turbulent energy dissipation rate can be evaluated numerically by solving the turbulence equations during CFD simulation or experimentally by measuring velocity fluctuations using, for example, hot wire anemometry, Laser Doppler Anemometry (LDA) or Particle Image Velocimetry (PIV). It is,

however, difficult to exactly estimate the turbulence energy dissipation rate a priori without numerical calculations or experimental work due to the complex nature of turbulent flow.
The total energy release rate from gas into liquid per unit mass of liquid may be calculated from changes in pressure energy and potential energy, as expressed by Dhotre and Joshi (2004) and Ekambara and Joshi (2005).

$$\varepsilon = \frac{U_G(\rho_L - \rho_G)g}{\rho_L} \tag{79}$$

This total energy release rate is partly converted into large scale liquid circulations and partly it is consumed by friction as gas bubbles move in the liquid.

When bubbles move in a liquid with a slip velocity u_S the energy dissipation rate may be calculated from the change in pressure and potential energy.

$$\varepsilon = \frac{(\rho_L - \rho_G)g\varepsilon_G u_S}{\rho_L} \tag{80}$$

If the bubble flow is in the turbulent regime ($Re > 500$) this energy dissipation rate is converted into turbulence in the vicinity of bubbles and finally spent in viscous dissipation. However, the turbulent eddies generated by the bubbles have a scale of bubbles, whereas the turbulence generated in the bulk liquid movement have a scale corresponding to the column dimensions. This issue has been discussed by Ekambra and Joshi and Dhotre and Joshi. They conclude that only a part of the turbulence generated by the bubbles will enter the bulk liquid motion and take part in the transport phenomena. This part is defined by a fraction C_B. The rest of the turbulence in small eddies is dissipated in the vicinity of the bubbles. Taking into account the fraction C_B the bubble induced turbulence is defined as

$$\varepsilon = C_B \frac{(\rho_L - \rho_G)g\varepsilon_G u_S}{\rho_L} \tag{81}$$

The rest of the total energy input rate expressed by Equation (80) is used to maintain liquid circulations and may be calculated as.

$$\varepsilon = \frac{(\rho_L - \rho_G) g (U_G - C_B \varepsilon_G u_S)}{\rho_L} \tag{82}$$

The energy rate for maintaining liquid circulations is also mainly converted into turbulence and finally consumed in viscous dissipation. However, a part of the energy rate is consumed by laminar shear near the column wall or is converted into small scale turbulence which does not enter the bulk liquid flow and is consumed by viscous dissipation.

When estimating the turbulent energy dissipation rate, it is necessary to consider several factors. The actual turbulent energy dissipation rate is lower than the total energy input rate because of column wall friction, energy consumed by laminar shear near bubbles for laminar flow (Re < 500) and energy consumed by small scale eddies near the bubble surface.

6. Estimation of volumetric mass transfer coefficient

In general, mass transfer between gas and liquid depends on several factors. These factors include the way the gas is inserted into the column or reactor (gas dispersion device), the volumetric flow rate of gas and liquid, geometry, flow arrangements (concurrent flow/countercurrent flow of phases), liquid physical properties, liquid composition, presence of impurities and gas density (or pressure). In three phase (slurry) columns the concentration and nature of the solid particles also affects gas-liquid mass transfer.

Due to the complex nature of the phenomenon, it is difficult to obtain a universal correlation for gas-liquid mass transfer in bubbly flows. Therefore, numerous experimental correlations for a volumetric mass transfer coefficient have been presented in the literature (for example, Akita and Yoshida, 1973; Nakanoh and Yoshida, 1980; Hikita et al., 1981; Öztürk, Schumpe and Deckwer, 1987). These correlations are usually obtained for model solutions at normal conditions, usually for oxygen in water at room temperature. Therefore, the general validity of the literature correlations is often questionable. Their validity is often limited to the chemical system and conditions used in the measurements and care should be taken in using these correlations in other conditions.

In this thesis, the volumetric mass transfer coefficient is estimated experimentally for three different gas-liquid columns. These are:

1) A bubble column with a T-junction two-phase-nozzle for gas dispersion (paper I). In a two-phase nozzle the kinetic and pressure energy is used to disperse gas into fine bubbles. A dynamic method is used to measure volumetric mass transfer coefficient. This method is based on measuring the concentration of dissolved gas as a function of time using a dissolved oxygen sensor.

2) A large scale industrial bubble column for oxidation of 2-ethyl tetrahydroanthrahydroquinone (paper II). An axial dispersion model in the form of a cell model with backmixing was written for the liquid phase and a steady state method was used to solve

concentration profiles of reactants in the column. Concentration profile data was available permitting estimation of volumetric mass transfer and axial dispersion coefficients.

3) A downflow concurrent bubble column with internal structured Katapak-S packing (Paper III). Plug flow was assumed for both phases and the volumetric mass transfer coefficient was estimated by comparing the measured and calculated dissolved oxygen concentration at the column outlet. The dissolved oxygen concentration was measured at the column inlet and outlet.

6.1 Bubble column with a T-junction nozzle for gas dispersion

Mass transfer between gas and liquid was studied in a bubble column where a T-junction two-phase nozzle was used to disperse the gas into fine bubbles. Two-phase nozzles, like the T-junction nozzle, use the kinetic energy of liquid and gas to disperse gas into fine bubbles. Kinetic energy is transferred into turbulence in the nozzle and finally lost in the column. The bubble column was operated as a semi-batch column, with a batch of liquid and continuous feed of gas through the column.

6.1.1 Experimental

Measurements were carried out in two different sizes of bubble columns. The smaller column had a diameter of 0.19 m. Three column heights were used. These were 0.67, 1.26 and 1.765 m. The larger column had a diameter of 0.97 m and a height of 4.64 m.

The volumetric mass transfer coefficient was measured in both columns using a dynamic step method. In the smaller column, the dissolved oxygen concentration was first lowered from saturation concentration by purging nitrogen into the column. When the oxygen concentration was less than 10 % of the saturation concentration, the nitrogen feed was stopped and the feed of air was started. In the larger column a dynamic pressure method proposed by Linek and Sinkule (1991) was used. In this method the pressure in the column is first increased temporarily by about 20 kPa. After saturation has been achieved, the pressure is suddenly reduced back to normal pressure. The changes in the dissolved oxygen concentration over

time were followed and recorded using a MARVET J40 oxygen sensor, which was located in the middle of the column. The sensor has a time lag of 4.5 -8 s depending on the age of the sensor.

A more detailed description of the experimental apparatus and the two-phase nozzles used is presented in paper I.

6.1.2 Mass transfer model

A model of mass transfer in the bubble column was developed using the following assumptions:

- a well-mixed liquid phase
- no depletion of oxygen concentration in the gas phase

The mass balance for oxygen in the liquid phase can be written as

$$V_R(1-\varepsilon_G)\frac{dc}{dt} = k_L A(c^* - c) \tag{83}$$

Dividing by $V_R(1-\varepsilon_G)$ gives

$$\frac{dc}{dt} = k_L \frac{A}{V_R(1-\varepsilon_G)}(c^* - c) = \frac{k_L a}{(1-\varepsilon_G)}(c^* - c) \tag{84}$$

After rearrangement

$$\frac{dc}{(c^* - c)} = \frac{k_L a}{(1-\varepsilon_G)}dt \tag{85}$$

Equation (85) can be integrated from initial concentration c_0 at $t = 0$ to concentration c at time t.

$$\int_{c_0}^{c} \frac{dc}{(c^* - c)} = \frac{k_L a}{(1-\varepsilon_G)}\int_0^t dt \tag{86}$$

After integration and rearrangement the following equation is obtained

$$k_L a = \frac{(1-\varepsilon_G)}{t} \ln\left(\frac{c^* - c_0}{c^* - c}\right) \tag{87}$$

An estimate for $k_L a$ can be obtained by fitting Equation (87) to the measured $c-t$ curve.

Possible sources of error in using Equation (87) for the estimation of $k_L a$ arise because of the model assumptions. Usually the assumption of ideal mixing is reasonable except for very tall and narrow columns. The assumption of insignificant depletion of oxygen concentration in the gas phase is acceptable if the mass transfer rate is not too high (see paper I for more details).

An additional error source comes from the use of dissolved oxygen sensors for the measurement of the oxygen concentration in the liquid phase. Because of their structure, these sensors have a time lag describing how fast they react to a change in liquid oxygen concentration. This time lag depends mainly on the physical and chemical properties and the thickness of the polymer film separating the studied liquid and the electrolyte solution inside the sensor head.

The probe time lag can be taken into account by using the following differential equation if the time lag is assumed to be first order with respect to time.

$$c = \frac{dc_m}{dt}\tau_p + c_m \tag{88}$$

Equation (88) can be used to correct the measured concentration c_m to the actual concentration c.

$$\frac{dc_m}{dt} = \frac{(c - c_m)}{\tau_p} \tag{89}$$

6.1.3 Results

The volumetric mass transfer coefficient was correlated to the jet kinetic power per nozzle volume using an empirical correlation form. It was found that a critical kinetic power per volume exists below which the nozzle does not disperse gas properly. Non-linear parameter

estimation gave the following correlation for the average volumetric mass transfer coefficient in the whole column for the studied column of height 1.765 m.

$$k_L a = 0.851 U_G^{0.942} \quad , \text{ for } (P_{kin} / V_{mix})_{cr} < 1945 \text{ W/m}^3 \qquad (90)$$

$$k_L a = 0.851 U_G^{0.942} \left(\frac{P_{kin}}{V_{mix}} \right)^{0.134} \quad , \text{ for } (P_{kin} / V_{mix})_{cr} > 1945 \text{ W/m}^3 \qquad (91)$$

where U_G is the volumetric mass transfer coefficient in m/s and $(P_{kin}/V_{mix})_{cr}$ is the critical kinetic power per mixing volume.

Kinetic energy per mixing volume is defined as

$$\frac{P_{kin}}{V_{mix}} = \frac{1}{2L_N} \rho_L U_{L,N}^3 \qquad (92)$$

where L_N is the nozzle length

The column was observed to be divided into two sections with different hydrodynamic and mass transfer characteristics. Near the nozzle, mixing and mass transfer were intensive. This section is called the spouting section and it has a height of 0.3 m. Above this section, mixing was less intensive (calm section). By using the measured data obtained with three column heights, the following correlation for the average volumetric mass transfer coefficient in the whole column was obtained

$$k_L a = 15.11 U_G^{0.87} \left(\frac{H_s}{H_{tot}} \left(\frac{P_{kin} / V_{mix}}{(P_{kin} / V_{mix})_{cr}} \right)^{0.33} + \frac{H_{tot} - H_s}{H_{tot}} \right), \qquad (93)$$

for $(P_{kin}/V_{mix})_{cr} > 1945$ W/m^3.

where H_s is the height of the spouting section (0.3 m) and H_{tot} is the total height of the column (1.765 m).

6.2 Large scale industrial bubble column with backmixing

The problem considered in this case was the oxidation of 2-ethyl tetrahydroanthrahydroquinone (THEAHQ) for the production of hydrogen peroxide. The oxidation is carried out in a large scale industrial bubble column operated concurrently with liquid and gas feed from the bottom of the column. In the column, oxygen is transferred from gas into liquid where it reacts with THEAHQ to produce 2-ethyl tetrahydroanhtraquinone (THEAQ) and hydrogen peroxide. Air is used as a source for the oxygen. The liquid phase is a mixture of organic solvents where all the reactants are dissolved. The oxidation reaction is assumed to be slow and to proceed in the bulk liquid phase.

Reaction kinetics is taken from Santacesaria et al. (1987).

$$r_{THEAHQ} = k_1 c_{THEAHQ}\, c_{O_2} \tag{94}$$

with the reaction rate constant $k_1 = 3.8 \times 10^{-3}$ m^3/mol s.

Because of the scale of the column, pressure varies in the column along the height as hydrostatic pressure decreases. Superficial gas velocity also changes because of changes in pressure and because the reaction consumes oxygen, which is transferred from gas phase.

The volumetric mass transfer coefficient and axial dispersion coefficient in the liquid phase were estimated from data obtained from the full-scale process. The data included oxygen concentration in the gas phase at the reactor outlet and hydrogen peroxide concentration at different locations along the reactor height.

Holdup was measured separately in laboratory scale in a bubble column with a diameter of 0.15 m. The liquid used in the measurement was the organic process solution at normal pressure and room temperature without reactants. The following correlation was obtained for gas holdup

$$\varepsilon_G = 0.642\, U_G^{0.294} \tag{95}$$

where U_G is in m/s.

The model used for parameter estimation is based on a cell model with backflow of both gas and liquid. The model consists of mass balance equations for model components in the gas and liquid phase and a momentum equation for each cell. Gas and liquid phase are connected to each other by mass transfer of model components in each cell. Different levels of model accuracy, plug flow of gas and ideally mixed liquid, axial dispersion in the liquid and gas phase, were considered with respect to process development. The cases studied and the results obtained are shown in Table 10. The estimated values for the volumetric mass transfer coefficient were comparable to literature data (see Figure 21).

6.2.1 Axial dispersion model

Before presenting the cell model, the equations of the traditional axial dispersion model are presented. A mathematical model for the bubble column describing convection, axial dispersion in phases, pressure difference, mass transfer and reaction in the steady state may be expressed by the following equations:

Momentum balance in the liquid phase

$$\frac{dp}{dz} = \left(\frac{dp}{dz}\right)_{dis} - g(\varepsilon_G \rho_G + \varepsilon_L \rho_L) \tag{96}$$

Total mass balance in the gas phase

$$\frac{dU_G}{dz} = -U_G \frac{1}{p}\frac{dp}{dz} - \frac{RT}{p}\sum_{i=1}^{N_{comp}} (k_L a)_i (c^*_{L,i} - c_{L,i}) \tag{97}$$

Mass balance of component i in the gas phase

$$\varepsilon_G E_G \frac{dc_{G,i}}{dz} = U_G \frac{dc_{G,i}}{dz} + c_{G,i}\frac{dU_G}{dz} + (k_L a)_i (c^*_{L,i} - c_{L,i}) \tag{98}$$

Mass balance of component i in the liquid phase

$$\varepsilon_L E_L \frac{dc_{L,i}}{dz} = z^* U_L \frac{dc_{L,i}}{dz} - (k_L a)_i (c^*_{L,i} - c_{L,i}) - \varepsilon_L \sum_{k=1}^{N_{comp}} \nu_{i,k} r_k \tag{99}$$

With

$$z^* = \begin{cases} +1 & \text{for concurrent gas/liquid flow} \\ 0 & \text{for semibatch operation} \\ -1 & \text{for countercurrent gas/liquid flow} \end{cases}$$

6.2.2 Cell model with backflow

A cell model with backflow has been presented by Mecklenburgh and Hartland (1975) and Schlüter, Steiff and Weinspach (1992) as an alternative way to solve the equations of the axial dispersion model. Basically, the cell model with backflow is a finite difference approximation of the axial dispersion model presented by Equations (96) – (99). The principle idea of the cell model can be seen in Figures 17 and 18. The column length is divided into a number of cells, which are connected to each other by the bulk flow of phases and the circulation between the cells. The amount of circulation depends on the axial dispersion in the column.

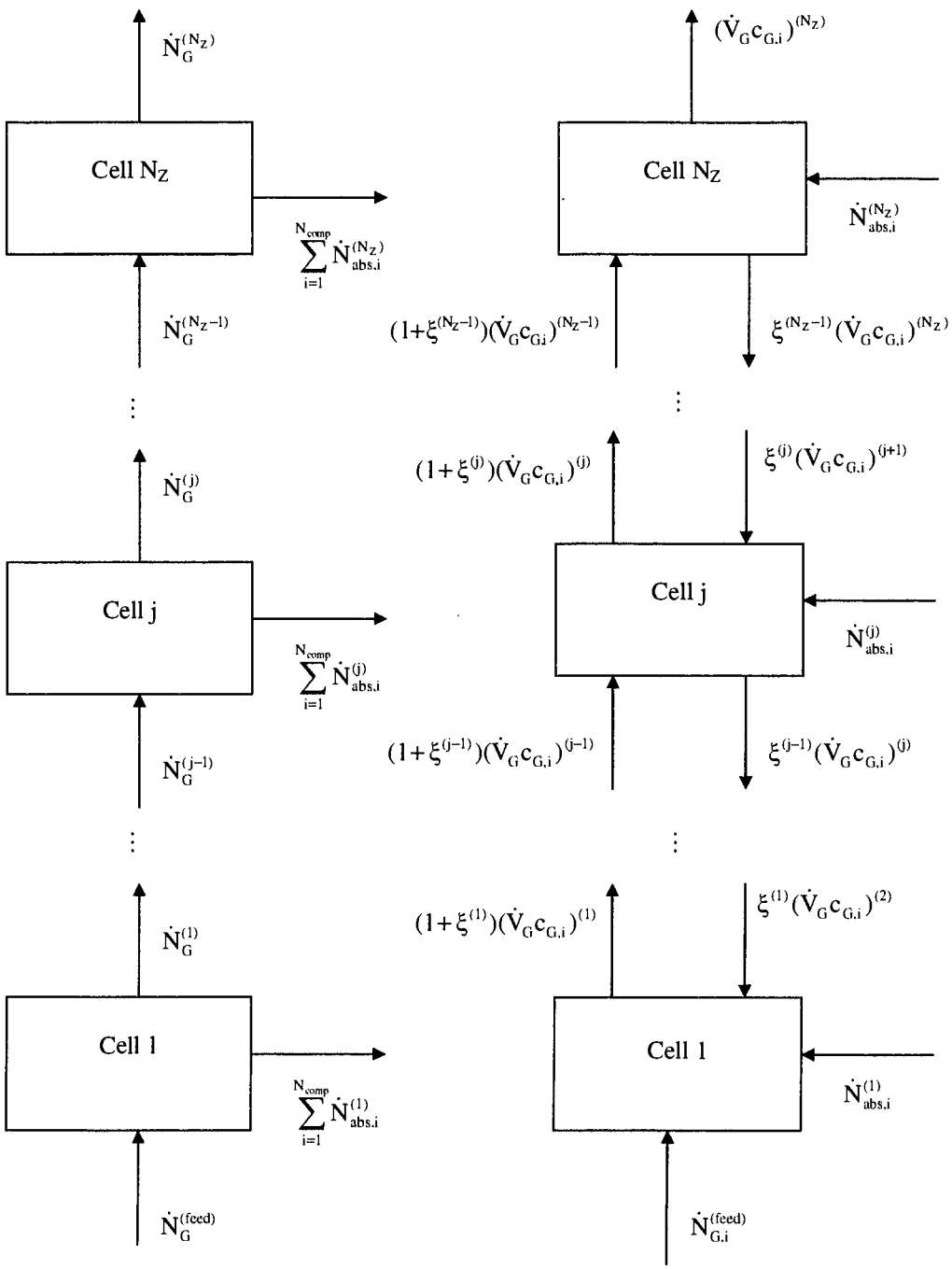

Figure 17. Mass balances for component i in the gas phase (on right) and total gas phase balance (on left) for the cell model with backflow according to Schlüter, Steiff and Weinspach (1992).

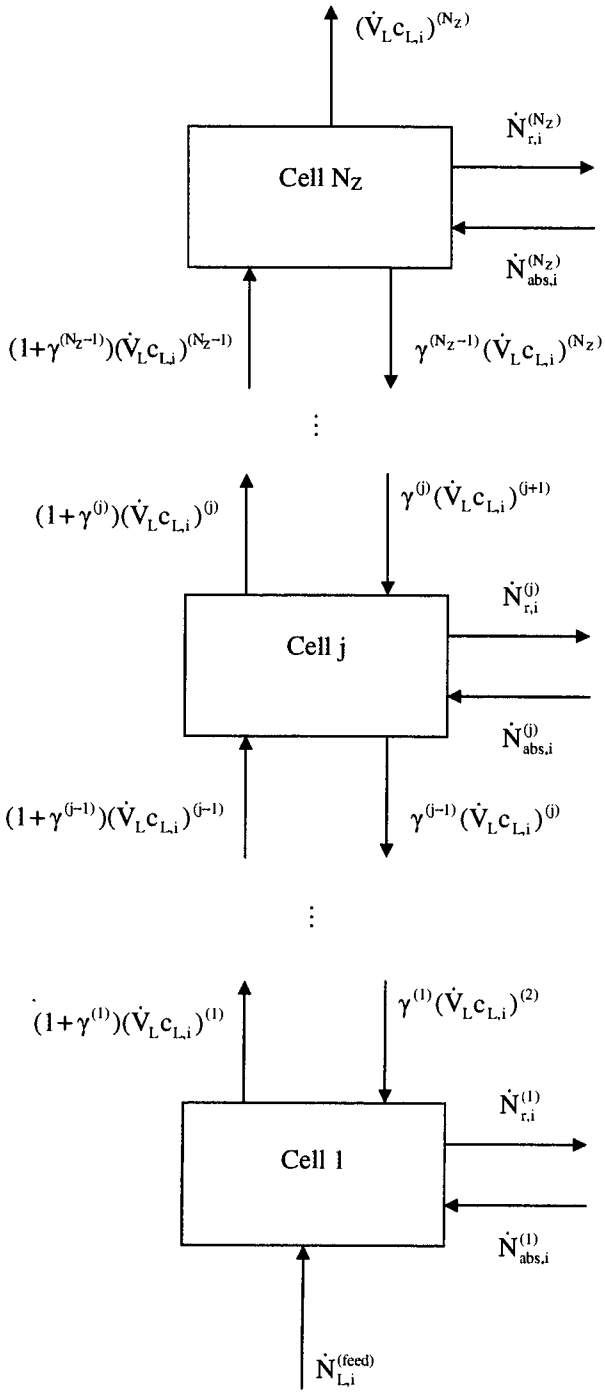

Figure 18. Mass balances for component i in the liquid phase for the cell model with backflow according to Schlüter, Steiff and Weinspach (1992).

Based on Figures 17 and 18 the following balance equations can be written for the cells from 1 (reactor bottom) to N_C (reactor top).

Momentum balances:

$$1 < j < N_C, \quad p_L^{(j)} - p_L^{(j+1)} \mp \frac{1}{2}(\Delta p_{diss}^{(j)} + \Delta p_{diss}^{(j+1)}) - \frac{g}{2}\left(H_C^{(j)}(\rho_G \varepsilon_G + \rho_L \varepsilon_L)^{(j)} + H_C^{(j+1)}(\rho_G \varepsilon_G + \rho_L \varepsilon_L)^{(j+1)}\right) = 0 \tag{100}$$

$$j = N_C, \quad p_L^{(N_C)} - p_{top} \mp \frac{\Delta p_{diss}^{(N_C)}}{2} - \frac{g H_C^{(N_C)}}{2}(\rho_G \varepsilon_G + \rho_L \varepsilon_L)^{(N_C)} = 0 \tag{101}$$

Liquid phase mass balances:

$$\text{For } j = 1, \quad \dot{N}_{L,i}^{Feed} + \gamma^{(1)} U_L c_{L,i}^{(2)} - (1+\gamma^{(1)}) U_L c_{L,i}^{(1)} + \frac{\dot{N}_{abs,i}^{(1)} - \dot{N}_{r,i}^{(1)}}{A_R} = 0 \tag{102}$$

$$\text{For } 1 < j < N_C, \quad (1+\gamma^{(j-1)}) U_L c_{L,i}^{(j-1)} - (1+\gamma^{(j)}) U_L c_{L,i}^{(j)} - \gamma^{(j-1)} U_L c_{L,i}^{(j)} + \gamma^{(j)} U_L c_{L,i}^{(j+1)} + \frac{\dot{N}_{abs,i}^{(j)} - \dot{N}_{r,i}^{(j)}}{A_R} = 0 \tag{103}$$

$$j = N_C, \quad (1+\gamma^{(N_C-1)}) U_L c_{L,i}^{(N_C-1)} - (1+\gamma^{(N_C-1)}) U_L c_{L,i}^{(N_C)} + \frac{\dot{N}_{abs,i}^{(N_C)} - \dot{N}_{r,i}^{(N_C)}}{A_R} = 0 \tag{104}$$

Gas phase mass balances:

$$j = 1, \quad \frac{\dot{N}_{G,i}^{Feed}}{A_C} + \xi^{(1)}(U_G c_{G,i})^{(2)} - (1+\xi^{(1)})(U_G c_{G,i})^{(1)} - \frac{\dot{N}_{abs,i}^{(1)}}{A_R} = 0 \tag{105}$$

$$1 < j < N_C, \quad (1+\xi^{(j-1)})(U_G c_{G,i})^{(j-1)} - (1+\xi^{(j)})(U_G c_{G,i})^{(j)} - \xi^{(j-1)}(U_G c_{G,i})^{(j)} + \xi^{(j)}(U_G c_{G,i})^{(j+1)} + \frac{\dot{N}_{abs,i}^{(j)}}{A_R} = 0 \tag{106}$$

$$j = N_C, \quad (1+\xi^{(N_C-1)})(U_G c_{G,i})^{(N_C-1)} - (1+\xi^{(N_C-1)})(U_G c_{G,i})^{(N_C)} - \frac{\dot{N}_{abs,i}^{(N_C)}}{A_R} = 0 \tag{107}$$

Total gas balance:

$$j=1, \qquad \frac{\dot{N}_G^{Feed}}{A_R} - \left(\frac{U_G p}{RT}\right)^{(1)} - \frac{1}{A_R}\sum_{i=1}^{N_{comp}} \dot{N}_{abs,i}^{(1)} = 0 \tag{108}$$

$$1<j<N_C, \qquad \left(\frac{U_G p}{RT}\right)^{(j-1)} - \left(\frac{U_G p}{RT}\right)^{(j)} - \frac{1}{A_R}\sum_{i=1}^{N_{comp}} \dot{N}_{abs,i}^{(j)} = 0 \tag{109}$$

Axial dispersion is taken into account with backflow of phases between the cells. The backflow ratio is calculated from the axial dispersion coefficient according to equations:

$$\xi^{(j)} = \frac{\dot{V}_{G,\xi}}{\dot{V}_G} = \frac{\dfrac{\bar{\varepsilon}_G E_G}{\Delta_\otimes U_G^{(j)}} \dfrac{\delta^{(j)}}{2}}{(1+\delta^{(j)})/2} \tag{110}$$

$$\gamma^{(j)} = \frac{\dot{V}_{L,\gamma}}{\dot{V}_L} = \frac{\dfrac{\bar{\varepsilon}_L E_L}{\Delta_\otimes U_L^{(j)}} \dfrac{\delta^{(j)}}{2}}{(1+\delta^{(j)})/2} \tag{111}$$

where $\Delta_\otimes$ is the mean cell height in the forward direction and δ is the backward/forward cell height ratio defined as

$$\Delta_\otimes = \frac{1}{2}(H_C^{(j)} + H_C^{(j+1)}), \tag{112}$$

$$\delta^{(j)} = \frac{H_C^{(j)} + H_C^{(j-1)}}{H_C^{(j)} - H_C^{(j+1)}} \tag{113}$$

Absorption rate is calculated from

$$\dot{N}_{abs,i} = k_L a\,(c_{L,i}^* - c_{L,i})\,V_C \tag{114}$$

and the reaction rate from

$$\dot{N}_{r,THEAHQ} = k_1 c_{THEAHQ}\, c_{O_2} V_C \tag{115}$$

The volumetric mass transfer coefficient is correlated to the superficial gas velocity by equation

$$k_L a = a_1 \left(\frac{U_G}{U_{G,mean}} \right)^{a_2} \tag{116}$$

and the axial dispersion coefficient in the liquid phase by equation

$$E_L = b_1 \left(\frac{U_G}{U_{G,mean}} \right)^{b_2} \tag{117}$$

where $U_{G,mean}$ is the mean superficial gas velocity with a value of 0.05 m/s.

Parameters a_1, a_2, b_1 and b_2 are experimental parameters, which can be obtained by solving the model equations and comparing the measured and calculated concentrations of hydrogen peroxide in the liquid phase and oxygen in the gas phase.

The number of the cells and the height of each cell in the model can be freely chosen, although at least three cells must be used. The cell model forms a group of nonlinear equations. The number of equations in the model is $2 \times N_{comp} \times N_C + N_C$, where N_{comp} is the number of components in the model and N_C is the number of cells. Model equations were solved numerically with the HYBRD1 routine from MINPACK software library routines (Garbow, Hillström and More, 1980). HYBRD1 is a modification of the Powell hybrid method. This routine chooses the correction as a convex combination of the Newton and scaled gradient directions and it is claimed to be globally convergent with almost all starting values.

6.2.3 Results

The results from the parameter estimation are presented in Table 10 and in Figures 19 and 20. Good agreement with the measured data and the calculated concentrations was obtained. When the predicted values for $k_L a$ are compared to a literature correlation (Akita and Yoshida, 1973) a reasonably good agreement can be seen at high gas superficial velocities. The estimated high exponent for superficial gas velocity in Equation (116) is probably attributed to the foaming nature of the liquid. According to the results from the sensitivity

analysis presented in Figures 22 and 23 the estimated parameters are well-identified and do not correlate to each other.

Table 10. Fitted model parameters with different reactor models (ADM = axial dispersion model, PF = plug flow, MF = ideally mixed flow).

Case	Liquid/Gas	a_1	a_2	b_1	b_2	R^2, %
A	PF/PF	0.0261	1.51	-	-	96.69
B	MF/PF	0.0334	2.73	-	-	96.91
C	ADM/ PF	0.0281	2.08	0.0884	1.0*	97.35
D	ADM/PF	0.0285	2.01	0.109	2.32×10^{-6}	97.41
E	ADM/PF	0.0285	2.01	0.11	0*	97.41

*) fixed value, not fitted

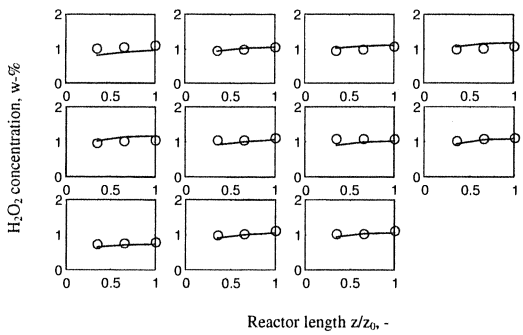

Figure. 19. Measured (o) and estimated (-) concentration profiles for H_2O_2 in an empty bubble column. Axial dispersion in the liquid phase, plug flow in the gas phase (Case E in Table 10).

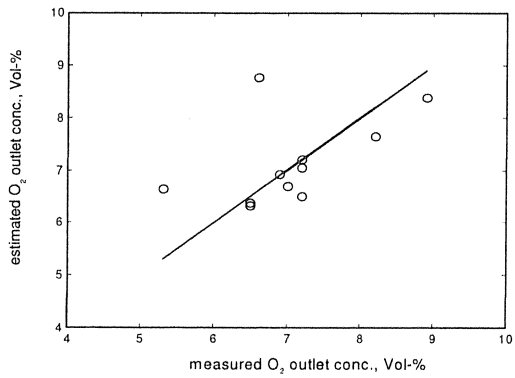

Figure. 20. Comparison of measured and estimated oxygen concentrations in the gas phase at reactor outlet. Axial dispersion in the liquid phase, plug flow in the gas phase (Case E in Table 10).

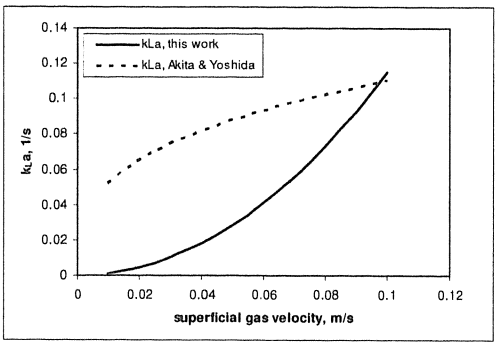

Figure 21. Comparison of the estimated volumetric mass transfer coeffcient and the correlation of Akita and Yoshida (1973).

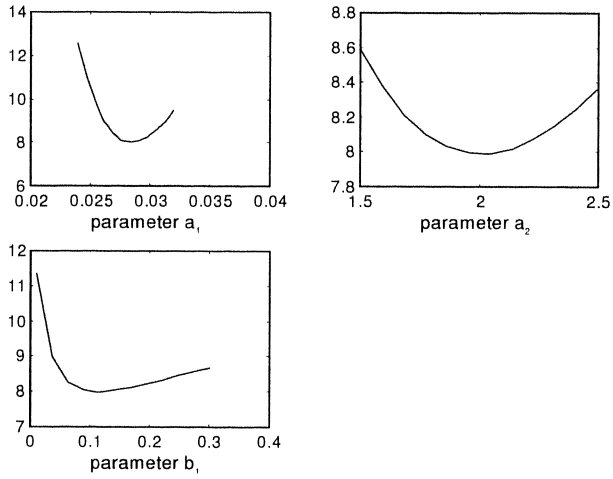

Figure 22. LSQ profiles for model parameters. Axial dispersion in the liquid phase, plug flow in the gas phase (Case E in Table 10).

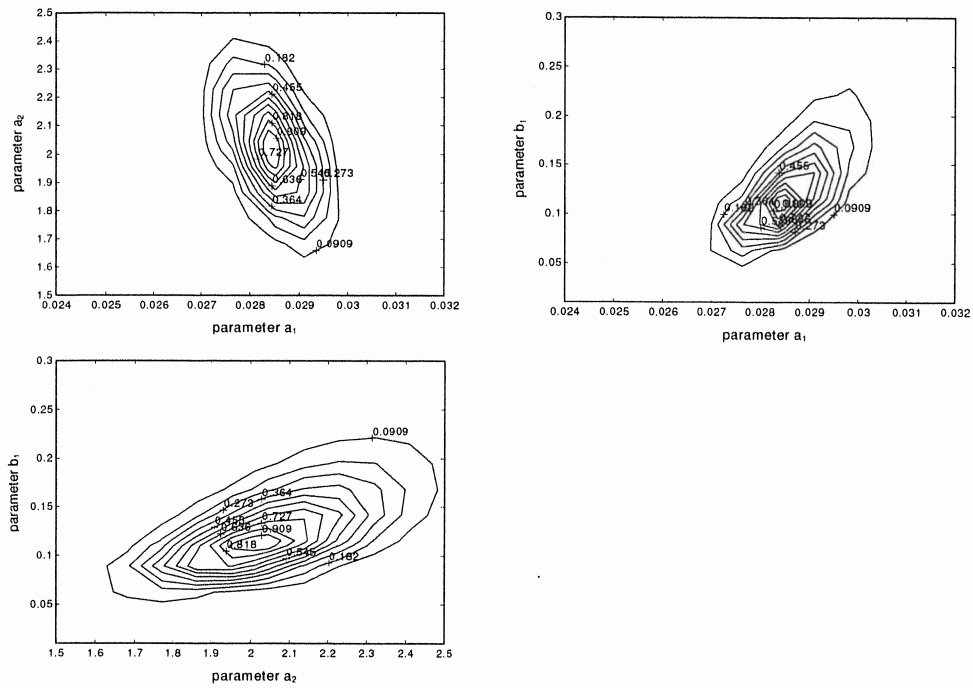

Figure 23. Sensitivity contour plot (R^2) for the parameters a_1, a_2 and b_1. Axial dispersion in the liquid phase, plug flow in the gas phase (Case E in Table 10).

6.3 Downflow structured packing

The volumetric mass transfer coefficient and gas holdup were estimated in a concurrent downflow gas-liquid column with an internal structured catalytic bed formed by Katapak-S elements (see Figure 24). The diameter of the column was 0.0849 m and its length was 2.35 m. The column was filled with 22 Katapak-S elements. Two different Katapak-S element types, the laboratory element (LE) and 500Y, were tested. Their characteristics are shown in Table 11.

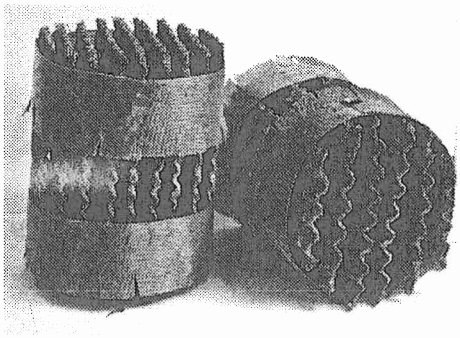

Table 11. Properties of the Katapak-S elements

Element type	Lab. element	500Y
Diameter, m	0.0849	0.0849
Contact angle, °	45	50
Wire, mm	0.25	0.25
Mesh, mm	0.5	0.5
Hydraulic diameter, mm	6.66	8.02
Element volume fraction	0.297	0.252
Stepsize, mm	12	10.2
Height of corrugation, mm	4	6.5
Surface/volume, m^2/m^3	300	250

Figure 24. Katapak-S elements.

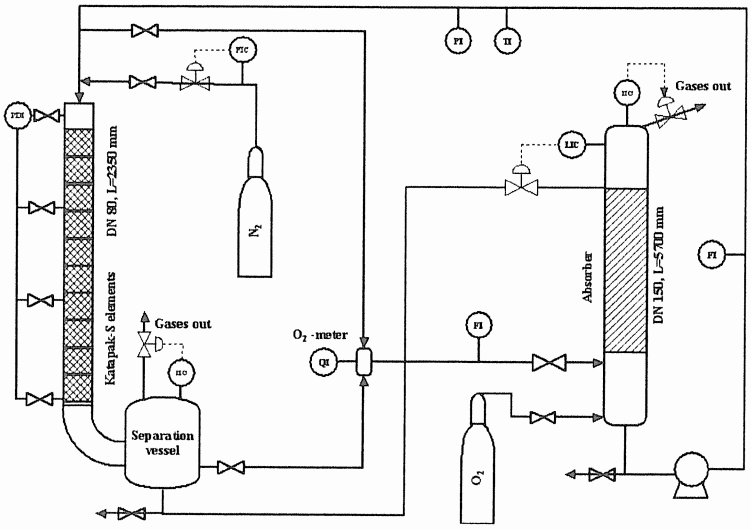

Figure 25. Experimental set-up for the measurement of mass transfer and gas holdup in Katapak reactors.

Estimation of $k_L a$ in a concurrent gas-liquid downflow column is based on a steady-state method where the dissolved oxygen concentration is measured simultaneously at steady state from the column inlet and outlet. Detailed description of the experimental apparatus is given in paper III.

6.3.1 Model

A model for pressure drop in the structured bed may be presented as follows. Total pressure drop is a sum of static and dynamic pressure drops. The expression for the dynamic pressure drop has been taken from Piironen, Haario and Turunen (2001).

$$\frac{dp}{dz} = -\frac{dp_{dyn}}{dz} + \frac{dp_{stat}}{dz} = \frac{\left(\frac{\alpha_p}{Re} + \beta_p\right)\rho_L U_L^2}{2d_H(1-\varepsilon_p)^2} + \rho_L g(1-\varepsilon_G) + \rho_G g \varepsilon_G \tag{118}$$

where α_p and β_p are experimental parameters.

The Reynolds number is defined as

$$Re_H = \frac{\rho_L d_H U_L}{\mu_L(1-\varepsilon_p)} \tag{119}$$

Assuming plug flow for gas and liquid, the differential mass balances for the gas phase components may be written as

$$\frac{d\dot{N}_{O_2}}{dz} = k_L a(c^*_{O_2} - c_{O_2})(1-\varepsilon_p) \tag{120}$$

$$\frac{d\dot{N}_{N_2}}{dz} = k_L a \frac{D_{N_2}}{D_{O_2}}(c^*_{N_2} - c_{N_2})(1-\varepsilon_p) \tag{121}$$

The volume in $k_L a$ is defined as the total volume of gas and liquid, excluding the volume of packings.

Similarly for the liquid phase

$$\frac{dc_{O_2}}{dz} = k_L a(c^*_{O_2} - c_{O_2})(1-\varepsilon_p)\frac{1}{\dot{V}_L} \tag{122}$$

$$\frac{dc_{N_2}}{dz} = k_L a \frac{D_{N_2}}{D_{O_2}}(c^*_{N_2} - c_{N_2})(1-\varepsilon_p)\frac{1}{\dot{V}_L} \tag{123}$$

The gas superficial velocity can be calculated from the total molar flow.

$$U_G = \frac{(\dot{N}_{O_2} + \dot{N}_{N_2})RT}{pA_R} \tag{124}$$

6.3.2 Results

The volumetric mass transfer coefficient and gas holdup were correlated to the liquid and gas superficial velocities using the following empirical correlation forms.

$$\varepsilon_G = a_1 \left(\frac{U_L}{U_{L,mean}} \right)^{a_2} \left(\frac{U_G}{U_{G,mean}} \right)^{a_3} \tag{125}$$

$$k_L a = c_1 \left(\frac{U_L}{U_{L,mean}} \right)^{c_2} \left(\frac{U_G}{U_{G,mean}} \right)^{c_3} \tag{126}$$

The effect of gas and liquid velocities and liquid properties on the gas holdup and mass transfer is complex. An increase in liquid velocity will increase the pressure drop, turbulence and bubble breakage, increasing the interfacial surface area and mass transfer. Due to a lower rising velocity, small bubbles are, however, at the same time carried away from the column by liquid flow, which tends to decrease gas holdup, interfacial area and mass transfer. The overall effect on mass transfer depends on the liquid's coalescence properties.

The parameters in the Equations (125) and (126) were estimated by comparing the measured and calculated pressure drops and column outlet concentrations.

Table 12. The estimated parameter values in the Equation (125) for average gas holdup in the reactor.

Dispersion device/ liquid/ element type	a_1	a_2	a_3	R^2, %
Venturi/ tap water/ LE	0.134	0.666	-1.83	98.87
Ring/ tap water/ LE	0.0982	0.657	-2.03	98.88
Ring/ organic solution / LE*	0.0642	2.00	-1.50	99.78
Ring/ organic solution/ LE	0.0585	2.60	-1.72	99.62
Ring/ organic solution/ 500Y*	0.0989	1.94	0.429	99.90

*) no mass transfer in the experiments

Table 13. The estimated parameter values in the Equation (126) for the average volumetric mass transfer coefficient in the Katapak reactor.

Dispersion device/ liquid/ element type	c_1	c_2	c_3	R^2, %
Venturi/ tap water/ LE	0.463	0.667	0.428	98.87
Ring/ tap water/ LE	0.340	0.657	0.234	98.88
Ring/ organic solution/ LE	0.0487	2.62	-0.631	99.62
Ring/ organic solution/ 500Y	0.0712	2.01	1.15	99.59

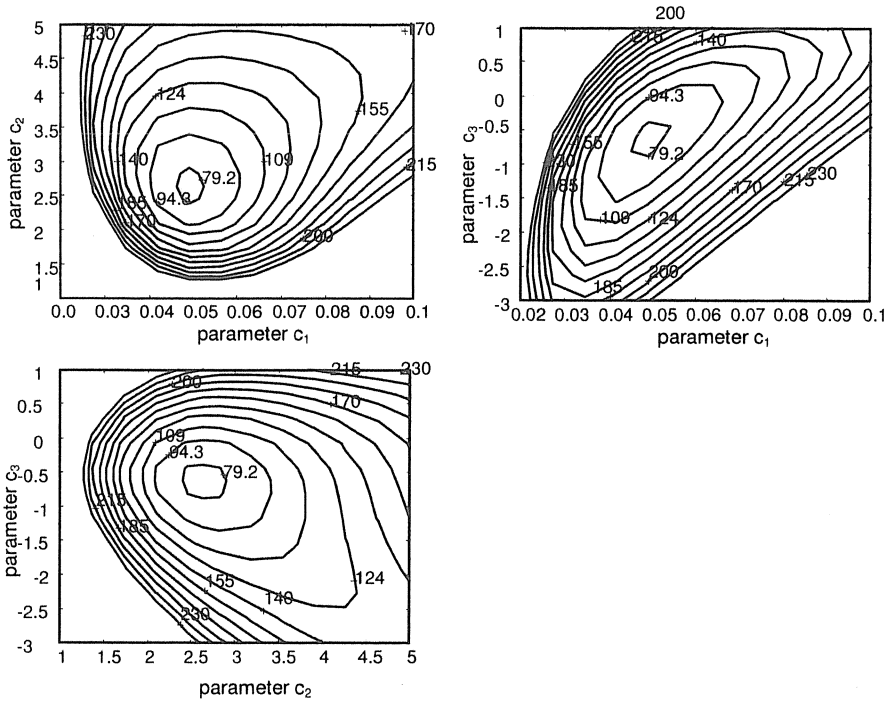

Figure 26. Sensitivity contour plots for the parameters c_1, c_2 and c_3 in the volumetric mass transfer coefficient equation (126), organic solution, ring sparger.

7. Conclusions

The subject of the present work is the estimation of mass transfer between gas and liquid in reactors and columns where the gas is flowing as bubbles in the liquid phase.

The problem has been approached in two ways. First, the volumetric mass transfer coefficient was estimated in gas-liquid reactors by measuring changes in the concentration of the absorbing component. This can be done either in a transient way by following changes of concentration in time, or in a steady-state way by recording local concentrations. This approach has been used in this thesis to estimate volumetric mass transfer coefficient and gas holdup in three different gas-liquid columns; a bubble column with a T-junction two-phase nozzle for gas dispersion, a large industrial scale bubble column for production of hydrogen peroxide, and a downflow gas-liquid column with internal structured catalytic bed.

In order to achieve as reliable and meaningful parameters as possible in the parameter estimation the sensitivity and identifiability of the parameters was also studied. This is an important issue in parameter estimation, which is usually not properly covered.

The main drawback of this traditional approach of measuring volumetric mass transfer coefficient is that the method gives only average mass transfer in the system. In addition, the estimated volumetric mass transfer coefficient is only reliable for the specific geometry and chemical system used in the measurements.

A more fundamental and accurate approach is to estimate bubble size distribution by the solution of population balance equations. The volumetric mass transfer coefficient can then be evaluated by using a theoretical or experimental mass transfer model, estimated bubble size distribution and measured gas holdup. Gas holdup can usually be measured easily and accurately. A novel idea is introduced for the calculation of theoretical mass transfer coefficient by applying simultaneously slip velocity and turbulent eddy concepts for the calculation of the surface renewal rate. The actual mass transfer coefficient depends also on interfacial surface mobility. The evaluation of interfacial surface mobility is, however, beyond the scope of this work.

Methods to estimate bubble size distributions were developed by solving population balance equations together with specific models for bubble breakage and coalescence. Parameters of breakage and coalescence models were estimated by comparing the measured and calculated bubble sizes. The drawback of this method is that the method is rather laborious since it requires the measurement of bubble size distributions in the column at several locations.

A method to estimate quantitatively coalescence properties by measuring the persistence time of a bubble at the free gas-liquid interface was developed. The varying coalescence properties of different solutions can be taken into account in coalescence models by replacing the film thinning or coalescence time by the measured persistence time. The obtained persistence times were compared with the coalescence times obtained from the bubble column measurements. For short persistence times, the persistence and coalescence times are in good agreement. For longer persistence times, however, the persistence times are at least an order of magnitude longer than the corresponding coalescence times from parameter fitting. This discrepancy may be attributed to the uncertainties concerning the estimation of energy dissipation rates, bubble-bubble collision rates and mechanisms and contact times of the bubbles.

8. References

Akita, K., Yoshida, F. (1973), Gas hold-up and volumetric mass transfer coefficient in bubble columns - Effect of liquid properties, *Ind. Eng. Chem. Process Des. Develop.*, **12**, 76-80.

Akita, K., Yoshida, F. (1974), Bubble size, interfacial area, and liquid-phase mass transfer area in bubble columns, *Ind. Eng. Chem. Process Des. Develop.*, **13**, 84-91.

Alves, S. S., Maia, C. I., Vasconcelos, J. M. T. (2004), Gas-liquid mass transfer coefficient in stirred tanks interpreted through bubble contamination kinetics, *Chem. Eng. Proc.*, **43**, 823-830.

Atkinson, B.W., Jameson, G.J, Nguyen, A.V., Evans, G.M., Machniewski, P.M. (2003), Bubble breakup and coalescence in a plunging liquid jet bubble column, *Can. J. Chem. Eng.*, **81** (3-4), 519-527.

Caldernak, P. H., Moo-Young, M. B. (1961), The continuous phase heat and mass transfer properties, *Chem. Eng. Sci.*, **16**, 39-61.

Chuang, K. T.-T., Strirling, A. J., Baker, J. C., An optical/electronic technique for measuring bubble coalescence times, *Ind. Eng. Chem. Fundam*, **23**, 109-113

Clift, R., Grace, J. R., Weber, M. E. (1978), Bubbles, drops and particles, Academic Press, New York.

Colella, D., Vinci, D., Bagatin, R., Masi, M., Abu Bakr, E. (1999), A study on coalescence and breakage mechanisms in three different bubble columns, *Chem. Eng. Sci.*, **54**, 4767-4777.

Deckwer, W.-D. (1992), Bubble column reactors, John Wiley & Sons, 1992.

Del Pozo, M., Briens, C. L., Wild, G. (1994), Efffect of organic liquid coalescing properties on mass transfer, heat transfer and hydrodynamics in a three-phase fluidized bed, *Chem. Eng. J.*, **55**, 1-14.

Dhotre, M. T., Joshi, J. B. (2004), Two-dimensional CFD model for the prediction of flow pattern, pressure drop and heat transfer coefficient in bubble column reactors, *Chem. Eng. Res. Des.*, **82**, 689-707.

Ekambara, K., Joshi, J. B. (2005), Computational fluid dynamics simulations in bubble-column reactors: Laminar and transition regime, *Ind. Eng. Chem. Res.*, **44**, 1413-1423.

Etchells, A.W., et al., A.I.Ch.E.J., Vol. 33 (1987), No. 4, pp. 663-667. Ref. Streiff, F.A., Käser, F., Sulzer mixer reactor SMR for gas/liquid reactions, 7th European Conference on Mixing, 1992, pp. 525-532.

Fleischer, C., Becker, S., Eigenberger, G. (1996), Detailed modeling of the chemisorption of CO_2 into NaOH in a bubble column, *Chem. Eng. Sci.*, **51**, 1715-1724.

Garbow, B., Hillström, K, More (1980), J., minpack –library, Argonne laboratory.

Garchia-Ochoa, F., Gomez, E. (2004), Theoretical prediction of gas-liquid mass transfer coefficient, specific area and hold-up in sparged stirred tanks, *Chem. Eng. Sci.*, **59**, 2489-2501.

Ghosh, P. (2004), Coalescence of air bubbles at air-water interface, Chem. Eng. Res. Des., **82**(A7), 849- 854.

Ghosh, P., Juvekar, V. A., (2002), Analysis of the drop rest phenomenon, *Chem. Eng. Res. Des.*, **80**, 715-728.

Gibilaro, L. G., Davies, S. N., Cooke, M., Lynch, P. M., Middleton, J. C. (1985), Initial response analysis of mass transfer in a gas sparged stirred vessel, *Chem. Eng. Sci.*, **40**, 1811-1816.

Grosz-Röll, von F., Bättig, J., Moser, F. (1983), Gas/Flüssig-Stoffübergang in statischen Mischern, Verfahrenstechnik, **17**, 698-707.

Haario, H. (1994), Modest User Manual, Profmath Oy, Helsinki.

Hagesaether, L., Jakobsen, H. A., Svendsen, H. F. (2002), A model for turbulent binary breakup of dispersed fluid particles, *Chem. Eng. Sci.*, **57**, 3251-3267.

Hagesaether, L. (2002), Coalescence and break-up of drops and bubbles, Ph.D. Thesis, University of Trondheim, Norway.

Hesketh, R. P., Russell, T. W. F., Etchells, A. W. (1987), Bubble size in horizontal pipelines, *AIChE J.*, **33**, 663-667.

Hesketh, R. P., Etchells, A. W., Russell, T. W. F. (1991), Bubble breakage in pipeline flow, *Chem. Eng. Sci.*, **46**, 1-9.

Hikita, H., Asai, S., Tanigawa, K., Segawa, K., Kitao, M. (1981), The volumetric liquid-phase mass transfer coefficient in bubble columns, *Chem. Eng. J.*, **22**, 61-69.

Hughmark, G. A., (1967), Holdup and mass transfer in bubble columns, *Ind. Eng. Chem. Proc. Des. Dev.*, **6**, 218-220.

Hörner, B., Abbenseth, R., Bergbauer, W. (1980), On the relationship between mass transfer and turbulence in gas absorption with chemical reaction, *Chem. Eng. Sci.*, **35**, 232-238.

Jamialahmadi, M., Müller-Steinhagen, H. (1992), Effect of alcohol, organic acid and potassium chloride concentration on bubble size, bubble rise velocity and gas hold-up in bubble columns, *Chem. Eng. J.*, **50**, 47-56.

Jordan, U., Terasaka, K., Kundu, G., Schumpe, A. (2002), Mass transfer in high-pressure bubble column with organic liquids, *Chem. Eng. Technol.*, **25**, 262-265.

Kamp, A. M., Chesters, A. K., Colin, C., Fabre, J. (2001), Bubble coalescence in turbulent flows: A mechanistic model for turbulence induced coalescence applied to microgravity bubbly pipe flow, *Int. J. Multiphase Flow.*, **27**, 1363-1396.

Kawase, Y., Halard, B., Moo-Young, M. (1987), Theoretical prediction of volumetric mass transfer coefficients in bubble columns for Newtonian and non-newtonian fluids, *Chem. Eng. Sci.*, **42**, 1609-1617.

Keitel, G., Onken, U. (1981), Errors in the determination of mass transfer in gas-liquid dispersions, *Chem. Eng. Sci.*, **36**, 1927-1932.

Keitel, G., Onken, U. (1982), Inhibition of bubble coalescence by solutes in air/water dispersions, *Chem. Eng. Sci.*, **37**, 1635-1638.

Kelkar, B. G., Godbole, S. P., Honath, M. F., Shah, Y. T., Carr, N. L., Deckwer, W.-D. (1983), Effect of addition of alcohols on gas holdup and backmixing in bubble columns, *A.I.Ch.E.J.*, **29**, 361-369.

Kim, J. W., Lee, W. K. (1987), Coalescence behaviour of two bubbles in stagnant liquids, *J. Chem. Eng. Japan*, **20**, 448-453.

Kumar, S., Ramkrishna, D. (1996), On the solution of population balance equations by discretization –I. A fixed pivot technique, *Chem. Eng. Sci.*, **51**, 1311-1332.

Laari, A., Kallas, J., Palosaari, S. (1997), Gas-liquid mass transfer in bubble columns with a T-junction nozzle for gas dispersion, *Chem. Eng. Technol.*, **20**, 550-556.

Laari, A., Turunen, I. (2003), Experimental determination of bubble coalescence and break-up rates in a bubble column reactor, *Can. J. Chem. Eng.*, **81** (3-4), 395-401.

Laari, A., Turunen, I. (2005), Prediction of coalescence properties of gas bubbles in a gas liquid reactor using persistence time measurements, *Chem. Eng. Res. Des.*, **83** (A7), 881-886.

Lara Márques, A. L., Wild, G., Midoux, N. (1994), A review of recent chemical techniques for the determination of the volumetric mass transfer coefficient k_La in gas-liquid reactors, *Chem. Eng. Proc.*, **33**, 247-260.

Lau, R., Peng, W., Velazquez-Vargas, L. G., Yang, G. Q., Fan, L.-S. (2004), Gas-liquid mass transfer in High-Pressure Bubble Columns, *Ind. Eng. Chen. Res.*, **43**, 1302-1311.

Lehr, F., Mewes, D. (2001), A transport equation for the interfacial area density applied to bubble column, *Chem. Eng. Sci.*, **56**, 1159-1166.

Lehr, F., Millies, M., Mewes, D. (2002), Bubble-size distributions and flow fields in bubble columns, *AIChE J.*, **48**, 2426-2443.

Lemoine, R., Behkish, A., Morsi, B. I. (2004), Hydrodynamic and mass-transfer characteristics in organic liquid mixtures in a large-scale bubble column reactor for the toluene oxidation process, *Ind. Eng. Chem. Res.*, **43**, 6195-6212.

Levich, V. G. (1962), Physicochemical hydrodynamics, Prentice Hall, 1962.
Lin, T.-J., Tsuchiya, K., Fan, L.-S. (1998), Bubble flow characteristics in bubble columns at elevated pressure and temperature, *AIChE J.*, **44**, 545-560.

Linek, V., Vacek, V. (1981), Chemical engineering use of catalyzed sulfite oxidation kinetics for the determination of mass transfer characteristics of gas-liquid contactors, *Chem. Eng. Sci.*, **36**, 1747-1768.

Linek, V., Sinkule, J. (1991), The influence of gas and liquid axial dispersion on determination of kLa by dynamic method, *Chem. Eng. Res. Des.*, **69**(A4), 308-12.

Linek, V., Sinkule, J., Benes, P. (1992), Critical assessment of the dynamic double-response method for measuring k_La: Experimental elimination of dispersion effects, *Chem. Eng. Sci.*, **47**, 3885-3894.

Linek, V., Benes, P., Sinkule, J., Moucha, T. (1993), Non-ideal pressure-step method for k_La measurements, *Chem. Eng. Sci.*, **48**, 1593-1599.

Linek, V., Kordač, M., Fujasová, M., Moucha (2004), T., Gas-liquid mass transfer coefficient in stirred tanks interpreted through models of idealized structure of turbulence in the bubble vicinity, *Chem. Eng. Proc.*, **43**, 1511-1517.

Luo, H., Svendsen, H. F. (1996), Theoretical model for drop and bubble breakup in turbulent dispersions, *AIChE J.*, **42**, 1225-1233.

Machoň, V., Vlček, J., Zahradník, J., Fialová, M. (1996), The effect of surface active substances on hydrodynamics and mass transfer in aerated stirred tank reactors, Proceedings of the 12th International Congress of Chemical and Process Engineering (CHISA 1996), Praha, Czech Republic, 25-30 August, 1996.

Marrucci, G. (1969), A Theory of Coalescence, *Chem. Eng. Sci.*, **24**, 975-985.

Mecklenburgh, J. C., Hartland, S. (1975), *The theory of backmixing*, Wiley, Bristol.

Moritz, P., Hasse, H. (1999), Fluid dynamics in reactive distillation packing Katapak-S, *Chem. Eng. Sci.*, **54**, 1367-1374.

Nakanoh, M., Yoshida, F. (1980), Gas absorption by newtonian and non-newtonian liquids in a bubble column, *Ind. Eng. Chem. Process Des. Dev.*, **19**, 190-195.

Oels, U., Lücke, J., Buchholz, R., Schügerl, K. (1978), Influence of gas distributor type and composition of liquid on the behaviour of a bubble column bioreactor, *Ger. Chem. Eng.*, **1**, 115-129.

Oolman, T., Blanch, H.W. (1986), Bubble Coalescence in Air-Sparged Bioreactors, *Biotech. Bioeng.*, **28**, 578-584.

Piironen M., Haario H., Turunen I. (2001), Modelling of Katapak reactor for hydrogenation of anthraquinones, *Chem. Eng. Sci.*, **56**, 859-864.

Prince, M.J., Blanch, H.W. (1990), Bubble coalescence and break-up in air-sparged bubble columns, *AIChE J.*, **36**, 1485-1499.

Pöpken, T., Geissler,R., Götze, L., Brehm, A., Moritz, P., Gmehling, J. (1999), Reaction kinetics and reactive distillation - on the transfer of kinetic data from a batch reactor to a trickle bed reactor, *Chem. Eng. Technol.*, **21**, 401-404.

Ramkrishna, D. (2000), Population balances – Theory and applications to particulate systems in engineering, Academic Press, 2000.

Rodrigue, D. (2001), Generalized correlation for bubble motion, *A.I.Ch.E.J.*, **47**, 39-44.

Santacesaria, E., Ferro, R., Ricci, S., Carra, S. (1987), Kinetic Aspects in the Oxidation of Hydrogenated 2-ethyltetrahydroanthraquinone, *Ind. Eng. Chem. Res.*, **26**, 155-159.

Schlüter, S., Steiff, A., Weinspach, P.-M. (1992), Modeling and simulation of bubble column reactors, *Chem. Eng. Process.*, **31**, 92-117.

Schäfer, R., Merten, C., Eigenberger, G. (2002), Bubble size distributions in a bubble column reactor under industrial conditions, *Exp. Therm. Fluid Sci.*, **26**, 595-604.

Streiff, F.A., Käser, F. (1992), Sulzer mixer reactor SMR for gas/liquid reactions, 7th European Conference on Mixing, 525-532.

Streiff, F.A., Mathys, P., Fischer, T.U. (1977), New Fundamentals for Liquid-Liquid Dispersion Using Static Mixers, 9th European Conference on Mixing, 9-12 March, 1977, Paris.

Ueyama, K., Saeki, M., Matsukata, M., Development of system for measuring bubble coalescence time by using a laser, *J. Chem. Eng. Japan*, **26**, 308-314.

Walter, J. F., Blanch, H. W. (1986), Bubble break-up in gas-liquid bioreactors: break-up in turbulent flows, *Chem. Eng. J.*, **32**, B7-B17.

Wang, T., Wang, J., Jin, Y. (2003), A novel theoretical breakup kernel function for bubbles/droplets in a turbulent flow, *Chem. Eng. Sci.*, **58**, 4629-4637.

Wang, T., Wang, J., Jin, Y. (2004), An efficient numerical algorithm for "A novel breakup kernel function of bubble/droplets in a turbulent flow", *Chem. Eng. Sci.*, **59**, 2593-2595.

Wilkinson, P. M., van Schayk, A., Spronken, J. P. M., van Dierendonck, L. L. (1993), The influence of gas density and liquid properties on bubble breakup, *Chem. Eng. Sci.*, **48**, 1213-1226.

Wilkinson, P.M., Haringa, H., van Dierendonck, L. L. (1994), Mass transfer and bubble size in a bubble column under pressure, *Chem. Eng. Sci.*, **49**, 1417-1427.

Yagi, H., Yoshida, F. (1974), Oxygen absorption in fermentors – Effects of surfactants, antifoaming agents and sterilized cells, *J. Ferment. Technol.*, **52**, 905-916.

Zahradník, J., Fialova, M., Kaštánek, F., Green, K. D., Thomas, N. H. (1995), The effect of electrolytes on bubble coalescence and gas holdup in bubble column reactor, *Chem. Eng. Res Des.*, **73**, 343-346.

Öztürk, S., Schumpe, A., Deckwer, W.-D. (1987), Organic liquids in a bubble column: Holdups and mass transfer coefficients, *A.I.Ch.E.J.*, **33**, 1473-1480.